10804–10823 *Nucleic Acids Research, 2016, Vol. 44, No. 22* *Published online 5 October 2016*
doi: 10.1093/nar/gkw861

Single-molecule analysis of ϕC31 integrase-mediated site-specific recombination by tethered particle motion

Hsiu-Fang Fan[1,2,*], Tao-shih Hsieh[3], Chien-Hui Ma[4] and Makkuni Jayaram[4]

[1]Department of Life Sciences and Institute of Genome Sciences, National Yang-Ming University, 112, Taiwan, [2]Biophotonics and Molecular Imaging Research Center, National Yang-Ming University, 112, Taiwan, [3]Institute of Cellular and Organismic Biology Academia Sinica, 115, Taiwan and [4]Department of Molecular Biosciences, University of Texas at Austin, Austin, TX 78712, USA

Received June 17, 2016; Revised September 11, 2016; Accepted September 22, 2016

ABSTRACT

Serine and tyrosine site-specific recombinases (SRs and YRs, respectively) provide templates for understanding the chemical mechanisms and conformational dynamics of strand cleavage/exchange between DNA partners. Current evidence suggests a rather intriguing mechanism for serine recombination, in which one half of the cleaved synaptic complex undergoes a 180° rotation relative to the other. The 'small' and 'large' SRs contain a compact amino-terminal catalytic domain, but differ conspicuously in their carboxyl-terminal domains. So far, only one serine recombinase has been analyzed using single substrate molecules. We now utilized single-molecule tethered particle motion (TPM) to follow step-by-step recombination catalyzed by a large SR, phage ϕC31 integrase. The integrase promotes unidirectional DNA exchange between *attB* and *attP* sites to integrate the phage genome into the host chromosome. The recombination directionality factor (RDF; ϕC31 gp3) activates the excision reaction (*attL* × *attR*). From integrase-induced changes in TPM in the presence or absence of gp3, we delineated the individual steps of recombination and their kinetic features. The gp3 protein appears to regulate recombination directionality by selectively promoting or excluding active conformations of the synapse formed by specific *att* site partners. Our results support a 'gated rotation' of the synaptic complex between DNA cleavage and joining.

INTRODUCTION

Site-specific recombinases have been classified as SRs and YRs, based on whether they utilize an active site serine or tyrosine as the nucleophile for DNA strand cleavage (1,2). These enzymes bring about a variety of genetic rearrangements (DNA integration, inversion, excision and translocation) via strand cleavage and exchange between specific target sites. The chemical steps of recombination are performed by four recombinase subunits, two associated with each core target site. As the strand cleavage and joining steps follow transesterification chemistry, recombination is completed in a conservative fashion without the requirement of exogenous energy input. SRs and YRs have served as valuable model systems for understanding the mechanisms and mechanics of phosphoryl transfer during site-specific recombination (3). Because of their strict target specificity, these recombinases have been developed as tools for directed genome engineering (4–8).

SRs and YRs differ strikingly in the chemical mechanisms of the cleavage/joining reactions and in the dynamics of exchanging the cleaved strands (1,2). The SRs form a 5′-phosphoserine linkage during cleavage, exposing a free 3′-hydroxyl group. By contrast, the cleaved intermediate formed by YRs is comprised of a 3′-phosphotyrosine bond and a 5′-hydroxyl group. During strand joining, the hydroxyl groups perform nucleophilic attack on the phospho-amino acid bonds in a cross-partner fashion. SRs make concerted double strand breaks in DNA. Biochemical, topological and structural evidence suggests that the cleaved complex goes through a 180° relative rotation, bringing the DNA ends in alignment for strand joining in the recombinant mode (9–13). YRs make single strand cuts, and complete recombination in two temporally distinct steps (3,14). The first cleavage/exchange step generates a Holliday junction; an analogous second step resolves this intermediate into reciprocal recombinant products. A simplified view of serine recombination is presented in Figure 1A.

The SRs contain a characteristic catalytic domain, present predominantly at the amino-terminus, which has been named the SR domain (2). The SR domain is attached, at the carboxyl-terminus in most cases, to a second domain

*To whom correspondence should be addressed. Tel: +886 2 28267941; Fax: +886 2 28234898; Email: hffan2@ym.edu.tw

© The Author(s) 2016. Published by Oxford University Press on behalf of Nucleic Acids Research.
This is an Open Access article distributed under the terms of the Creative Commons Attribution License (http://creativecommons.org/licenses/by-nc/4.0/), which permits non-commercial re-use, distribution, and reproduction in any medium, provided the original work is properly cited. For commercial re-use, please contact journals.permissions@oup.com

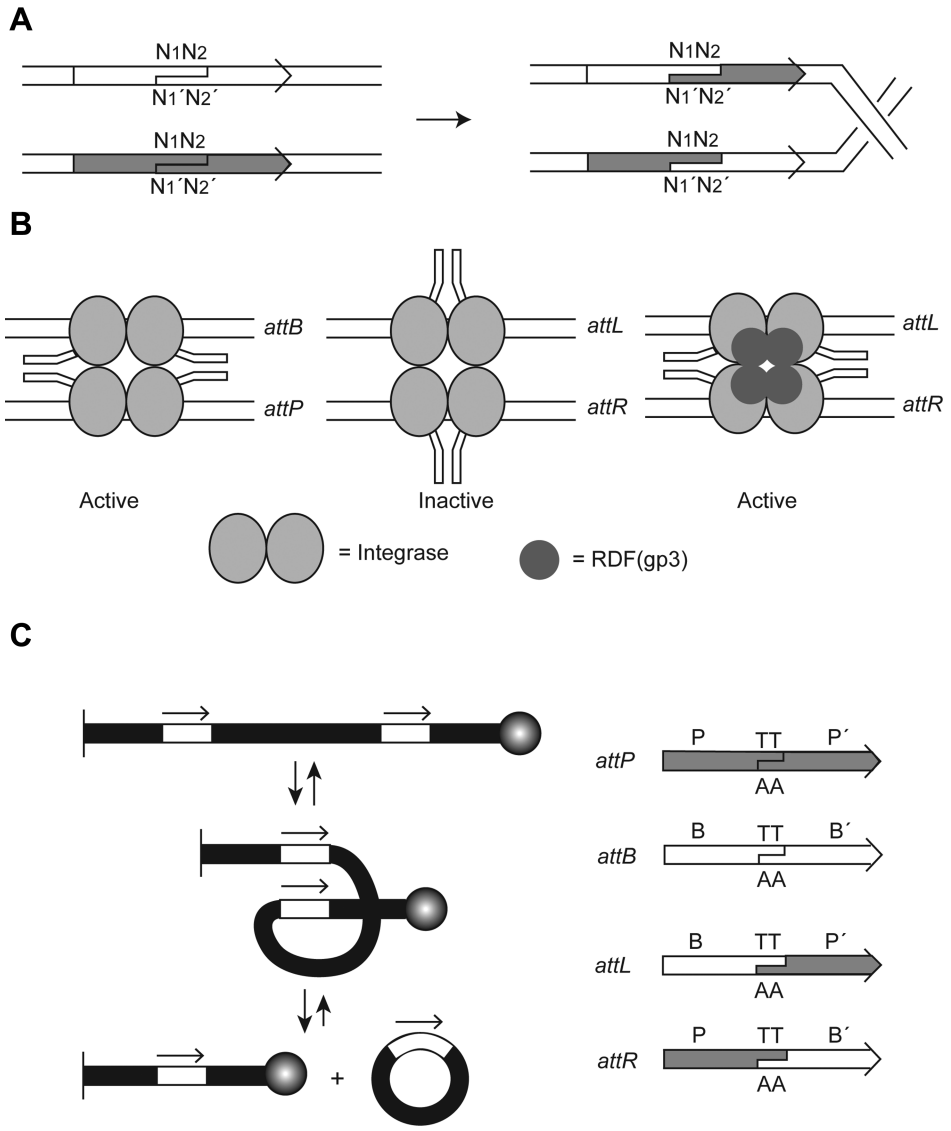

Figure 1. Recombination by serine phage integrases. (**A**) The general reaction mechanism for SRs is schematically diagrammed. The partner sites aligned in parallel undergo double strand cleavage, 180° relative rotation and strand joining in the recombinant mode. The central dinucleotides sandwiched between the scissile phosphates, and exchanged during recombination, are indicated as $N_1N_2/N_1'N_2'$. (**B**) The directionality of phage-coded serine integrases (large SRs) in recombination (*attB* × *attP* = integration; *attL* × *attR* = excision) is dictated by recombination directionality factors (RDFs). They appear to act by promoting the functional synaptic conformation between *attL* and *attR*, while blocking *attB* and *attP* from assuming this conformation. The simplified representations of the active and inactive synaptic forms shown here are based on the recently proposed structural model (36). Interaction of the coiled-coil motifs (CCs; drawn as peptide extensions) between integrase dimers bound to partner *att* sites induces the active synapse. Interaction of the CCs within integrase dimers bound to each *att* site leads to an inactive synapse. The RDF for ϕC31 integrase is the phage protein gp3. (**C**) The ϕC31 integrase reaction between two *att* site partners (rectangular boxes) placed in head-to-tail orientation in a liner DNA is schematically outlined at the left. The relative orientation of the sites is indicated by the direction of the arrows above them. In this and subsequent similar schematic figures, the surface and the bead to which the DNA ends are attached for tethered particle motion (TPM) assays are shown by a line and a sphere, respectively. The recombinant products are a linear molecule and an excised circle. The *att* sites employed in this study are schematically represented at the right. Assays were performed on the *attB-attP* pair or the *attL-attR* pair in the presence of the integrase or integrase plus the gp3 protein. All but one set of reactions, with *attB-attP* sites in head-to-head orientation, employed partner sites in head-to-tail orientation.

which can vary significantly in size, sequence and properties among individual recombinases. The well-studied transposon resolvases and invertases belong to the small SR family, characterized by a small helix-turn-helix (HTH) DNA binding carboxyl-terminus. In the large SR family, the HTH domain is replaced by considerably larger (300–500 amino acids long) carboxyl-terminal extensions. A subgroup of this family comprises phage-coded serine integrases, including the integrase of the *Streptomyces* phage ϕC31 (15,16).

ϕC31 integrase and other phage serine integrases differ from the tyrosine integrases of λ and λ-related phage in the shorter length and simpler organization of the phage recombination target site *att*P (17–20). The *attP* sites of the tyrosine integrases contain binding sites for accessory factors coded for by the bacterial host (IHF, Fis) as well as

the phage (Xis). These proteins regulate the choice between lysogeny and lysis by channeling Int recombination toward phage integration or excision. By contrast, the functional *attP* and *attB* (the target site on the bacterial chromosome) sites for the ϕC31 integrase are quasi-symmetric and ≤50 bp in length, with roughly 30% sequence similarity between the two. The *attB* × *attP* reaction, responsible for phage integration, results in the formation of asymmetric *attL* and *attR* as the recombinant sites flanking the integrated DNA. The excision reaction (*attL* × *attR*) is activated only in the presence of the phage-encoded gp3 protein, a recombination directionality factor (RDF) (21). This regulatory feature of ϕC31 integrase makes it an attractive tool in one-way genome engineering and editing applications. Control of recombination directionality toward integration or excision by RDFs appears to be a general feature of serine recombinases encoded by phage and prophage-like elements (22–24).

The tyrosine recombinases λ Int, Cre and Flp have been extensively investigated in single DNA molecules by fluorescence energy transfer and tethered particle motion (TPM) approaches (25–30). TPM is particularly simple and efficient in monitoring the individual steps of recombination, as it conveys the changes in DNA length associated with these steps as corresponding changes in the Brownian motion amplitude (BM amplitude) of a polystyrene bead attached to one end of the DNA. Earlier TPM analyses demonstrated subtle thermodynamic and kinetic differences among λ Int, Cre and Flp recombinases within the context of their overall mechanistic similarities (25,27,29). Similar studies using active site mutants of Cre and Flp revealed unsuspected roles for the conserved catalytic pentad of YRs in the pre-chemical steps of recombination (26).

There has been only one reported study of the action of a serine recombinase, the integrase of the mycobacteriophage Bxb1, on single DNA molecule substrates (31). The constrained DNA substrates, with negative supercoils incorporated into them, were designed to report on DNA cleavage, completion of recombination or return to the parental state by supercoil relaxation, loss of DNA tether or restoration of torsional stress, respectively. The results obtained with this large SR generally support the subunit rotation model inferred from previous studies of small SRs (9–13). However, a somewhat surprising finding from the tethered single-molecule DNA substrates or from braided pairs of DNA substrates was the long open state of the cleaved synaptic complex, permitting multiple rounds of rotation between DNA cleavage and joining. Prior topological results suggest that processive recombination by SRs, more than one round of recombination without dissociation of the original synapse, does occur but is infrequent. The unconstrained rotation observed with the Bxb1 integrase is either an exception to the general behavior of topologically selective small SRs or an artefact induced by the reaction conditions employed. A more recent analysis of recombination by ϕC31 integrase performed from the topologically well-defined Tn3 resolvase synapse suggests a gated rotation model with one round of rotation, rather than multiple rounds, between DNA cleavage and joining (32).

A long-standing question concerns the regulation of site-selectivity by large SRs during synaptic assembly and the consequent directionality of recombination. The prevailing view that conformational changes in the integrase subunits directed by the DNA sequences of partner sites determine their synaptic compatibility (33–35) is now supported by the structure of the carboxyl-terminal domain of *Listeria* phage integrase bound to its *att*P half-site (36). A recombinase domain (RD) and an unusual zinc ribbon domain (ZD) linked to it interact extensively with *att*P, while a coiled coil motif (CC) present between helices in ZD extends away from the main protein–DNA complex. The CC motifs from juxtaposed half-sites are positioned to interact favorably to form only *attB*-*attP* synapsis, while excluding *attP*-*attP* or *attB*-*attB* synapsis. The interactions of the CC motifs derived from the *attB* and *attP* half-sites position *attL*- and *attR*-bound ZDs in an auto-inhibited complex, thus blocking *attL*-*attR* synapse formation. Presumably, the RDF proteins promote the reconfiguration of the inhibitory complex to permit functional *attL*-*attR* pairing. The available DNA binding and recombination data from recombinase and *att* site mutants are consistent with this architectural model for functional synapsis suggested by the structure (36–39). The implications of the model for regulation of recombination directionality via alternative synaptic conformations are illustrated in Figure 1B.

We have now applied single-molecule TPM for analyzing ϕC31 integrase recombination stepwise, examining gp3-regulated switch in recombination directionality, distinguishing active synapses from inactive ones and addressing the rotational freedom of the cleaved synaptic complex. The salient findings are presented in this report.

MATERIALS AND METHODS

Proteins

The ϕC31 integrase and gp3 proteins were expressed in *Escherichia coli*, and purified according to published procedures (21,35).

DNA substrates

The *att* site-containing plasmids were constructed in the PL451 vector (obtained from ATCC). The *attB* or the *attL* site was cloned between the SalI and BspEI sites of the vector. The *attP* or *attR* site was inserted between the BssHII and BamHI sites. The sequences of the *att* sites are listed in Supplementary Table S1.

The 1303 bp long recombination substrates and control molecules with a single *att* site were prepared by PCR amplification of PL451-derived plasmids containing *attB*-*attP*, *attL*-*attR*, *attB* or *attP* (Supplementary Tables S1 and S2). A 551-bp mimic of the linear excision product of *attB* × *attP* recombination was obtained from the plasmid containing head-to-tail *attL*-*attR*. For preparing the 1303-bp control DNA without an *att* site, the template was pBR322 DNA. The primer pair in each PCR reaction contained a 5′-digoxigenin label in one and a 5′-biotin label in the other (Supplementary Tables S1 and S2).

Single-molecule TPM measurement and data analysis

One end of the DNA molecules was anchored on a glass cover slip by digoxigenin-anti-digoxigenin interac-

tions. These molecules were tethered at the other end to polystyrene beads (200 nm in diameter) by biotin–streptavidin interactions. The details of the TPM analysis, including reaction chambers, sample preparation and the criteria for eliminating aberrantly behaved molecules from data analysis have been previously described (25,40). All data presented here were smoothed using a five-point adjacent averaging algorithm. The BM amplitude values are expressed as the Mean ± 2 × SD (95% confidence limit).

In the figures depicting the TPM data (Figure 3–7), BM amplitude changes in DNA molecules from a typical experiment are shown in panel **A**. The dwell time plots for individual DNA–protein complexes (panels **B** and **C**) were based on the cumulative data from five to seven repetitions of the experiment. For dwell time estimates of the complexes prior to synapsis of *att* sites, only the initial events (conversion of a substrate molecule to the protein-bound form for the first time) were counted. For all other dwell times, multiple transition events that a single-molecule undergoes (as recorded by the BM amplitude time traces) were taken into account. The N-values in the dwell time histograms (Figures 3–7) comprise a subset of transition events randomly chosen from the recorded time traces.

The dwell time histograms were fit to a single exponential algorithm ($y = A_1 \times e^{(-k1 \times t)}$) in all cases except one, where a double exponential algorithm was employed ($y = A_1 \times e^{(-k1 \times t)} + A_2 \times e^{(-k2 \times t)}$). The fitting parameters were determined by the Origin 8.0 software.

The goodness of fit was $0.92 \leq R^2 \leq 1.0$.

Recombination reactions

The reaction chamber (22°C) containing the tethered DNA molecules was buffered with 10 mM Tris-HCl, pH = 8.0, 100 mM NaCl, 4.5% glycerol, 5 mM dithiothreitol and 1 mg/ml bovine serum albumin. ϕC31 integrase (5 nM), alone or together with the gp3 protein (20 nM), was added in the same buffer to initiate the reaction. At the end of the 30 min incubation period, 100 μl of 0.05% sodium dodecyl sulfate (SDS) in the reaction buffer was flowed into the chamber to quench the reaction.

The choice of 5 nM concentration of integrase, which is close the 5–20 nM K_d reported in the absence of ethylene diamine tetraacetic acid (41), was based on standardization assays. At this concentration, integrase binding to *att* sites was optimal for TPM observations without nonspecific DNA association and without causing molecules to stick to the surface. Under the reaction conditions employed, the two *att* sites present within a substrate were occupied by integrase in a sufficient number of molecules, as revealed by their progression to the synapsed state.

At 0.05% SDS concentration, the attachment of the DNA molecules to the glass surface or to the polystyrene bead was not affected. At the same time, as revealed by experimental observations, DNA–protein and protein–protein interactions relevant to the steps of recombination were disrupted. In recombination-blocked reactions, following SDS treatment, nearly all protein-bound molecules shifted to the high BM amplitude of the DNA substrate. The dislodgement of DNA-bound proteins by SDS was further verified by individual post-SDS time traces that did not show the fluctuations expected from the transitions that protein-bound molecules undergo.

SalI treatment of tethered DNA molecules

The DNA molecules were tethered to the glass surface in the reaction chamber containing the SalI digestion buffer (from New England BioLabs). SalI (20 units; New England BioLabs) was introduced into the chamber in the same buffer. The detachment of the beads from DNA was monitored by following the BM amplitude time traces.

RESULTS

Rationale of the single-molecule TPM analyses of recombination by ϕC31 integrase

The majority of *attB* × *attP* or *attL* × *attR* reactions analyzed in the present study are schematically represented in Figure 1C. The TPM assays were performed in 1303 bp long DNA molecules containing partner *att* sites arranged in head-to-tail orientation and tethered to a glass surface at one end. The changes in DNA length associated with the pre-chemical steps or the completion of recombination were recorded by the Brownian motion (BM) amplitude of a polystyrene bead attached to the other end (25,27). The binding of integrase to the *att* sites and the resulting conformational constraints caused a measurable shortening (intermediate BM amplitude) of the DNA (Figure 2A; top). A larger reduction in length (low BM amplitude) occurred upon synapsis of the bound *att* sites, with looping of the intervening DNA. The effect was the same for successful recombination, causing the excision of a 752 bp circle and shortening the tethered DNA to 551 bp. Synapsis could be distinguished from recombination by SDS-mediated protein dissociation from DNA. Whereas synapsed (but unrecombined) molecules returned to the substrate length, recombined molecules stayed short (Figure 2A; bottom). For one set of experiments, the relative *attB-attP* orientation was reversed without changing their locations (or their spacing) within the 1303 bp substrate. In a typical TPM experiment (e.g. Figure 3A), the measured high, intermediate and low BM amplitudes were 95.3 ± 14.4 nm (substrate), 63.9 ± 6.8 nm (*att* sites bound by integrase) and 44.3 ± 12.4 nm (*att* sites bound and synapsed by integrase), respectively. The same general pattern was observed in other experiments, containing integrase or integrase plus gp3, as well (Figures 4–7), with only small variations in the mean BM amplitudes of these species.

BM amplitude changes induced by integrase or integrase plus gp3 in DNA standards designed to provide a frame of reference in the TPM assays are summarized in Supplementary Figures S1 and S2 and Supplementary Table S3. Note that protein association with a single *att* site did not produce a reliable shift in BM amplitude (Supplementary Figure S1; Supplementary Table S3). As a result, the measured BM amplitude changes represent the occupancy of both *att* sites of a substrate and the subsequent transitions that these bound molecules undergo.

The distinct types of the pre-chemical integrase-*att* site complexes revealed by TPM in single-molecule time traces

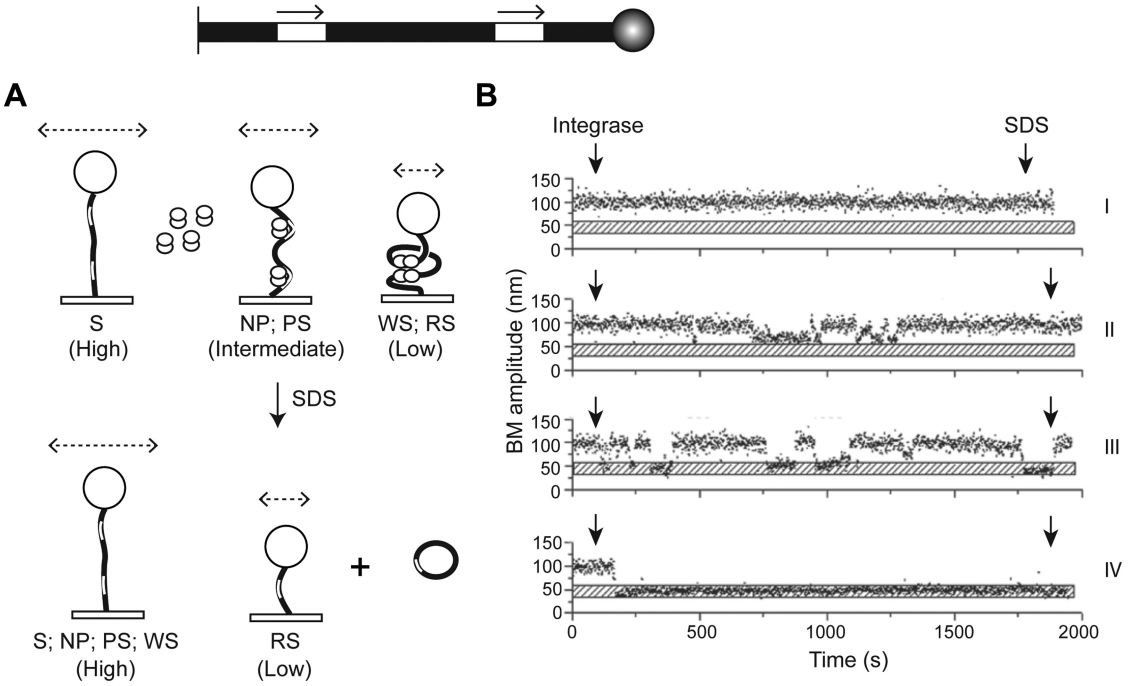

Figure 2. TPM analysis of integrase-*att* site complexes and integrase-mediated recombination between *att* sites. The tethered DNA substrate (1303 bp) containing *attP* and *attB* sites in head-to-tail orientation is drawn schematically at the top. The spacing between the *att* sites was 752 bp. A subset of the analyses utilized an analogous DNA substrate containing *attL* and *attR* sites. In one set of assays, the *attB-attP* orientation was reversed (head-to-head). (**A**) The Brownian motion amplitude (BM amplitude) of the bead (shown as a sphere) attached to the tethered DNA is 'high' in the protein-free DNA substrate (S). Binding of integrase dimers (paired ovals) to the *att* sites decreases the BM amplitude to an 'intermediate' value. The complexes formed are non-productive (NP) or pre-synaptic (PS). Pairing of the *att* sites results in the 'low' BM amplitude of the wayward synaptic (WS) complexes or recombinogenic synaptic (RS) complexes. PS-complexes may also arise by dissociation of the synapse in WS-complexes (see Figure 10 and Table 1). When the *att* sites are stripped of the bound integrase by SDS addition, the RS-complexes remain in the low BM amplitude state, as they have completed recombination to yield the tethered 551 bp linear recombinant plus the excised free 752 bp circular product. All other complexes show the high BM amplitude of the substrate. The dashed lines with arrowheads at either end denote relative BM amplitudes. In some of the assays, which included integrase plus the gp3 protein, the general changes in the BM amplitude patterns were similar to those shown here. The properties of the individual complexes (NP, PS and RS) are explained in Table 1 and in the text. (**B**) Typical time traces illustrating the behavior of individual molecules are shown. (I) This trace represents a substrate (S) molecule that was not bound by integrase during the observation period. (II) In this case, integrase binding produced the NP complex that transitioned between the bound and protein-free (substrate) states. (III) Shown here is a molecule that gave the WS- complex following integrase binding. The BM amplitude fluctuations in this recombination-incompetent complex corresponded to multiple events of synapse dissociation and reformation (WS → PS →WS) or synapse dissociation followed by protein dissociation (WS → PS → S). (IV) Synapsis of the *att* sites in this molecule resulted in the RS-complex, successful in recombination. The horizontal stippled bars in I-IV indicate the BM amplitude consistent with the synapsis of *att* sites (see also Supplementary Figure S2). The time points for integrase or SDS addition are shown by short vertical arrows. Individual BM amplitude transitions occurring in quick succession could be clearly resolved by expanding the time axis.

(Figure 2A and B; Table 1) may be summarized as follows. The bound complexes either proceeded to form synapsis, or were blocked in this step. The former synapsis-competent molecules were called 'pre-synaptic complexes' (PS-complexes). The latter ('non-productive complexes'; NP-complexes) returned to the high starting BM amplitude, presumably by protein dissociation. Similarly, two types of synapsed molecules were detected. Those that went on to complete recombination were designated as 'recombinogenic synaptic complexes' (RS-complexes). Others, arrested between synapsis and recombination, were termed 'wayward synaptic complexes' (WS-complexes). Dissociation of the synapse in WS-complexes reverted them to PS-complexes, which fell into two subsets. In one, the synapse was reformed to give the WS- or RS-complexes. In the other, dissociation of bound proteins from the *att* sites followed de-synapsis to give substrate DNA.

Productive recombination follows the path: DNA substrates → PS-complexes → RS-complexes → recombinant products. The PS-, and NP- complexes display similar BM amplitudes; so do the RS- and WS-complexes prior to SDS treatment. The RS-complexes maintain the low BM amplitude state stably, while the WS complexes go through amplitude transitions. The off-pathway complexes, NP and WS, need not be dead-end complexes. They may enter the normal reaction path by transitioning to the PS-complex directly (WS → PS → RS) or to the substrate first and then to the PS-complex (NP → S → PS → RS; WS → PS → S → PS → RS). Based on the life-time of a given reaction state before its progression to a subsequent state or its reversal to a prior state, the kinetic constants for the individual reaction steps could be derived.

Recombination between *attB* × *attP*

Integrase-mediated recombination between *attB* and *attP* mimics the integration of phage DNA, the products of the reaction being *attR* and *attL*. In our substrate design, *attL*

Table 1. Bound complexes formed by *att* site association with integrase or integrase plus gp3. The names of the complexes, their abbreviations and their identifying features are summarized. Although the NP- and PS-complexes represent molecules with similar BM amplitudes containing unsynapsed *att* sites bound by integrase or integrase plus gp3, they can be distinguished by their transition paths under single-molecule observation. NP- and PS-complexes are formed initially from the substrate S, but differ in their subsequent fate, NP → S and PS → WS or RS. The WS-complexes are also the precursors of the PS-complexes, which may either re-synpase or dissociate to the substrate

Complexes formed by binding of integrase or integrase plus gp3 to *att* sites		Characteristics
Non-productive complexes	NP	Formed by protein binding to substrate. Revert to protein-free substrate.
Pre-synaptic complexes	PS	Formed by protein binding to substrate; proceed to synapsis. Also formed by synapse dissociation in WS-complexes; may re-synapse or may dissociate to substrate.
Wayward synaptic complexes	WS	Formed from PS-complexes by *att* site synapsis. Do not perform recombination. Dissociate to PS-complexes.
Recombinogenic synaptic complexes	RS	Formed from PS-complexes by *att* site synapsis. Carry out recombination.

and *attR* become separated into the linear and circular recombinant products, respectively.

Out of 131 DNA molecules containing head-to-tail *attB* and *attP* sites, 76 molecules with a starting BM amplitude = 95.3 ± 14.4 nm (Figure 3A-I) exhibited a lower BM amplitude in response to integrase addition during the 30 min assay period (Figure 3A-II). These were distributed into two populations. Five showed a BM amplitude of 63.9 ± 6.8 nm, likely representing molecules in which the *att* sites occupied by integrase were not synapsed (Supplementary Figure S1; Supplementary Table S1). In the larger set of 71 molecules with a BM amplitude of 44.3 ± 12.4 nm, *att* site synapsis or *attB* × *attP* recombination had occurred. Their BM amplitude matched that expected for the linear product of the excision reaction (Supplementary Figure S2). The high BM amplitude populations observed at 30 min incubation (Figure 3A-III) signify the dissociation of NP-complexes (unsuccessful in synapsis) and that of WS-complexes (unsuccessful in recombination) via PS-complexes (formed by synapse disassembly). Following SDS addition at 30 min (Figure 3A-IV), all complexes except the RS-complexes showed the high substrate BM amplitude, indicating a lack of recombination. Approximately half the synapsed molecules (46.5%) retained the low BM amplitude after SDS treatment, denoting successful recombination. Using a single exponential fit, the dwell times of the substrate and the observed complexes (Figure 3B and C) were converted to the kinetic constants for the individual steps of the reaction (Table 2).

Examples of the single-molecule time traces that provided the data for this experiment and similar experiments (Figures 4–7) are assembled in Supplementary Figure S3.

As a protein-free DNA molecule and one in which a single *att* site is protein-bound cannot be distinguished by their BM amplitudes, the dwell time measurements for the S → PS and S → NP association steps will include both the unbound substrate and singly bound molecules. An analogous limitation applies to the PS → S and NP → S dissociation steps as well. Here, the measured dwell times in the PS and NP states represent protein dissociation from one *att* site alone or from both the sites. Thus, concerted versus temporally distinct association or dissociation events are not differentiated in the kinetic analyses.

Action of ϕC31 integrase on head-to-tail *attL* and *attR* sites

Although integrase can bind to *attL* and *attR*, it fails to promote the association of the bound sites into a productive recombination synapse (21). As a result *attL* × *attR* recombination does not occur. The gp3 protein does not bind directly to *att* sites but interacts with integrase in solution or with *att*-bound integrase (21). Formation of stable *attL-attR* synapsis to trigger recombination is strongly dependent on gp3. We examined integrase-DNA binding and subsequent DNA dynamics in 1303 bp molecules containing *attL* and *attR* sites in head-to-tail orientation in the absence of gp3. The *attL-attR* spacing was the same as in the *attB-attP* substrate. In the event of recombination, the excised 752 bp circle would contain *attP*, with *attB* remaining in the 551 bp linear product.

Approximately 27% (32/119) of the substrate molecules (Figure 4A-I) showed a decrease in BM amplitude upon integrase addition, indicating DNA–protein association as well as *attL-attR* interactions (Figure 4A-II). The distribution of the lower BM amplitude was considerably broader than that seen in the *attB-attP* substrate, suggesting that integrase-induced conformations were heterogeneous. These molecules could be grouped into two roughly equal subpopulations, with mean BM amplitudes of 64.5 ± 6.4 nm and of 50.3 ± 10.2 nm. The higher value indicated a lack of synapsis; the lower one was consistent with synapsis. The shift in the distribution toward the high BM amplitude at 30 min (Figure 4A-III) resulted from synapse disassembly and protein dissociation occurring in a majority of the molecules. All molecules returned to the high amplitude state following SDS treatment (Figure 4A-IV), indicating that recombination was blocked (WS-complexes). Kinetic constants were derived by fitting the dwell times to a single exponential model (Figure 4B and C; Table 2).

The present results are in agreement with published gel mobility shift assays and biochemical data demonstrating the ability of integrase to bind *attL* and *attR* in the absence of gp3, without being able to recombine them (21). However, in contrast to the TPM findings, the earlier analyses did not detect synapsis of integrase bound *attL* and *attR*. It is possible that synaptic interactions were not strong enough to survive the conditions of gel electrophoresis. Our results suggest that integrase requires the assistance of gp3 to as-

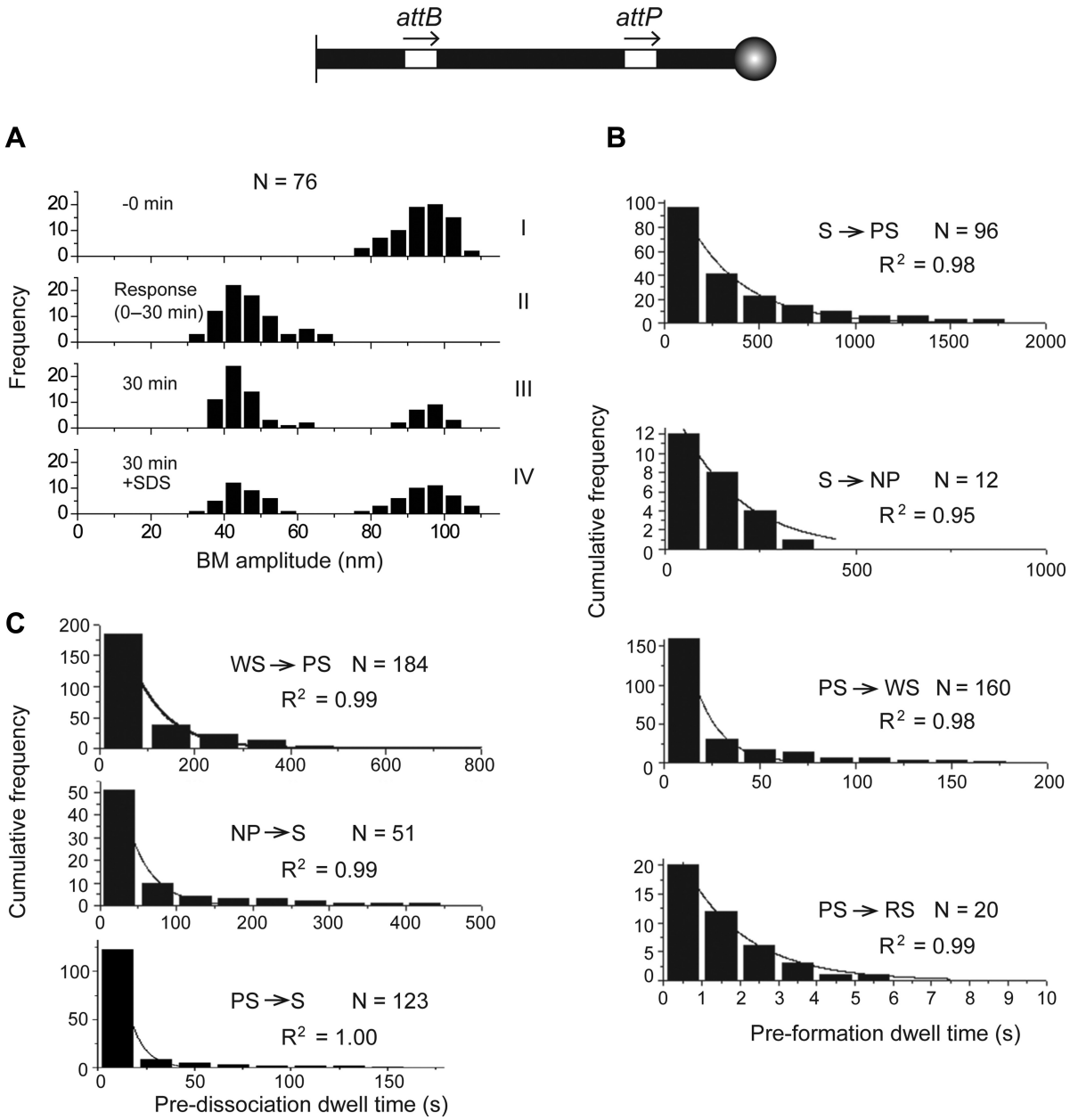

Figure 3. Characterization of *attB-attP* recombination by integrase in a substrate containing the sites in head-to-tail orientation. In the schematic representation at the top, the *att* sites and their relative orientation in the tethered DNA substrate are indicated as in Figure 2. (**A**) The BM amplitude distribution of single substrate molecules (N = 76) just prior to the addition of integrase (-0 min) are shown in the top panel (I). These molecules responded to integrase addition within the 30 min observation period, and shifted to lower BM amplitudes (II). The BM amplitude distributions at 30 min of incubation (just prior to SDS addition) and those following SDS addition were compiled in III and IV, respectively. (**B** and **C**) The following dwell times were plotted as histograms: (**B**) As substrate (S) before formation of NP-complexes (non-productive) or PS-complexes (pre-synaptic); as PS-complexes before conversion to WS-complexes (wayward synapses) or RS-complexes (recombinogenic synapses); (**C**) as WS-complexes before dissociation to PS-complexes and as NP-complexes or PS-complexes before reversal to protein-free substrate. Each N value in (**B**) and (**C**) is the number of events scored from single-molecule time traces recorded in a set of independent experiments. The general arrangement of panels in this figure is followed in Figures 4–7. Within a figure, the scale on the X-axis (frequencies) and that on the Y-axis (time) in the sub-panels of A are kept the same. In B and C, the scales differ, as the number of transition events counted and the dwell-times of individual complexes vary among the sub-panels.

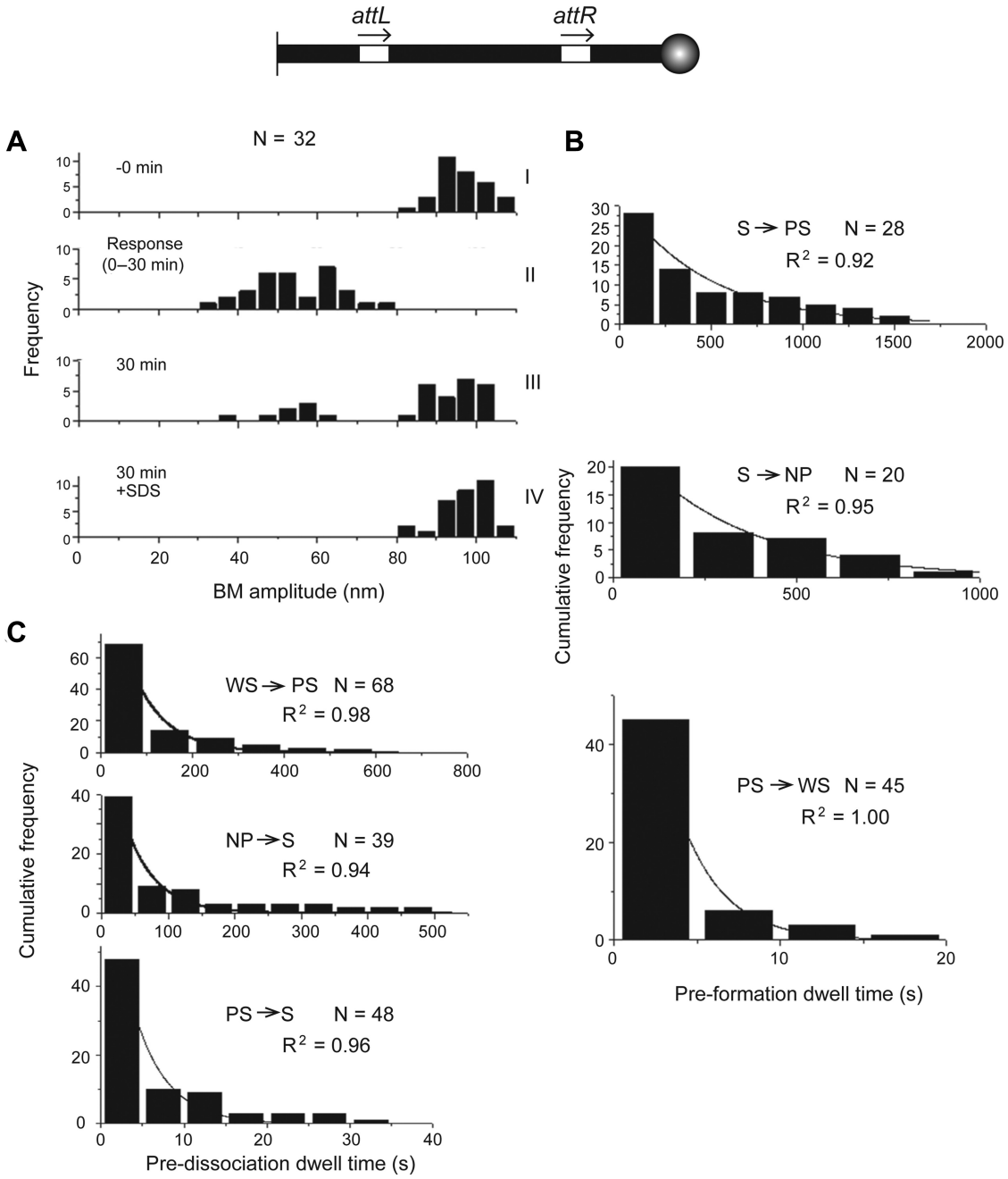

Figure 4. BM amplitude changes mediated by integrase in the DNA substrate containing *attL-attR* in head-to-tail orientation. (**A**) The BM amplitude distributions and the (**B** and **C**) dwell time histograms are arranged as in Figure 3. Note that in this assay there was no PS → RS conversion (absence of recombination).

semble *attL* and *attR* into a functional synapse or to reorganize a non-functional (wayward) synapse into a functional one (see Figure 1B).

Integrase-mediated *attL* × *attR* recombination facilitated by gp3

According to the current structural model, the failure of *attL* × *attR* recombination in the absence of gp3 results from the unfavorable interactions between the carboxyl-terminal CC motifs of adjacent integrase monomers within the synapse (16,36) (Figure 1B). CC interactions within the integrase dimer bound to each *att* site confer chemical incompetence on the synapse. The gp3 protein fosters CC interactions between neighboring integrase monomers across the *attL-attR* partners, thereby activating recombination. We followed the effects of gp3 alone or gp3 together with integrase on the *attL-attR* substrate in the TPM assay.

Consistent with the inability of gp3 to bind *att* DNA, addition of gp3 to the *attL-attR* containing DNA molecules did not result in a BM amplitude shift (Supplementary Figure S4A). However, the addition of integrase plus gp3 re-

Table 2. Kinetics of recombination between *att* sites mediated by integrase or integrase plus gp3. The rate constants were determined by fitting the dwell times shown in Figures 3–7 to a single exponential model, except for one step of the *attB-attP* inversion reaction (see below). The orientation of the *att* sites in a substrate is indicated by the direction of the arrows. The rate constants for formation of the complexes are: k-NP_f; k-PS_f; k-WS_f and kRS_f. The rate constants for their dissociation are: k-WS_d; k-PS_d and k-NP_d. The abbreviated names of the individual complexes and their properties are described in Table 1. For the reaction of the head-to-head *attB-attP* sites with integrase, the value for k-WS_d (marked by an asterisk) includes the rate of dissociation of the WS-complex as well as the conversion of the RS-complex into recombinant products (k_{rec}). As the RS- and WS-complexes could not be differentiated during *attB-attP* inversion, a double exponential model was used to fit the dwell times for the PS → RS/WS conversion to derive two rate constants. By comparison to the *attB-attP* deletion reaction, the higher and lower values were assigned to k-RS_f and k-WS_f, respectively

Reaction conditions		k-SP_f	k-NP_f x10^{-5} ($M^{-1}s^{-1}$)	k-RS_f x10^2 (s^{-1})	k-WS_f x10^2 (s^{-1})	k-WS_d x10^2 (s^{-1})	k-NP_d x10^2 (s^{-1})	k-DS_d x10 (s^{-1})
Integrase	attB-attP	6.9 ± 0.5	12.3 ± 2.1	62.5 ± 3.9	7.2 ± 0.8	1.4 ± 0.1	3.0 ± 0.2	1.3 ± 0.1
	attL-attR	4.3 ± 0.6	6.5 ± 1.0		3.8 ± 0.0	1.4 ± 0.2	2.2 ± 0.3	2.5 ± 0.4
	attB-attP	6.1 ± 0.5	3.6 ± 0.2	30.7 ± 3.7	4.0 ± 0.5	1.5 ± 0.1*	1.7 ± 0.2	5.6 ± 0.7
Integrase + gp3	*attB-attP*	3.3 ± 0.2	4.5 ± 0.4		16.9 ± 1.7	2.7 ± 0.2	3.5 ± 1.5	0.9 ± 0.1
	attL-attR	3.2 ± 0.2	2.4 ± 0.5	6.6 ± 1.0	45.5 ± 4.1	3.6 ± 0.2	6.5 ± 0.4	9.1 ± 0.8

vealed BM amplitude changes in 51 out of 113 molecules. The changes were consistent with the formation of NP-, PS- as well as WS- and/or RS-complexes (Figure 5A-I–III). Furthermore, molecules in the low BM state after SDS challenge confirmed the execution of recombination by RS-complexes (Figure 5A-IV). The kinetic constants for the individual reaction steps, obtained by single exponential fit to dwell times (Figure 5B and C), are assembled in Table 2.

The TPM results verify the conclusion reached from biochemical and structural studies (21,36) that a directionality factor influences recombination without directly interacting with *att* sites. Rather, its role is in modulating interactions among the pair of integrase dimers that contact the *att* sites.

Action of integrase plus gp3 on head-to-tail *attB-attP* sites

The gp3 protein controls directionality not only by promoting *attL-attR* recombination but also by inhibiting *attB-attP* recombination. In principle, gp3 may interfere with *attB-attP* synapsis, or induce a non-reactive conformation of the synapse. We tested how the presence of gp3, in addition to integrase, modulated the TPM behavior of the *attB-attP* substrate compared to integrase alone.

As was observed with the *attL-attR* substrate, addition of gp3 alone did not cause a down-shift in the BM amplitude of the *attB-attP* containing DNA (Supplementary Figure S4B). However, addition of integrase plus gp3 to a substrate population of 119 molecules brought about BM amplitude decreases in 26 of these (Figure 6A-I and II). The BM amplitude distribution in Figure 6A-II was bimodal, 58.5 ± 22.4 nm indicating protein association with the *att* sites and 39.7 ± 7.0 nm indicating synapsis. The predominance of the high BM amplitude distribution at 30 min (Figure 6A-III) was consistent with the instability of the synapse and with dissociation of the bound proteins. The pattern was similar to that observed for the *attL-attR* sites treated with integrase in the absence of gp3 (Figure 4A-III). Following SDS treatment, the high BM amplitude was restored in all molecules except two (Figure 6A-IV). It is possible that these molecules underwent recombination as they were bound by integrase but not gp3. Alternatively, a small fraction of the *att* sites might be functionally synapsed by integrase even in the presence of gp3. A trivial possibility is that the low BM amplitude was an artifact caused by DNA sticking to the glass surface. Although we cannot ascertain the reason for the persistent low BM amplitude, a low level

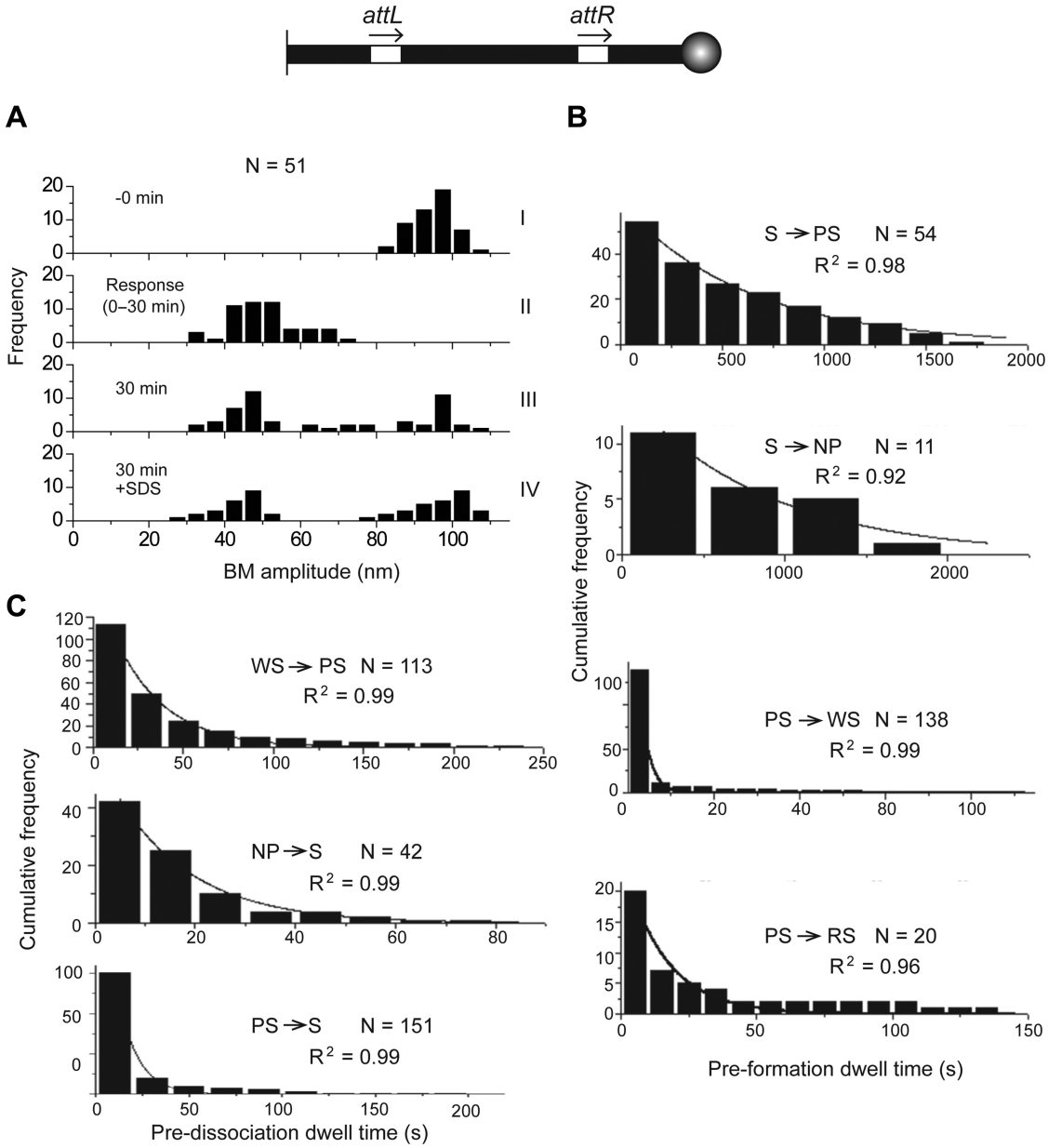

Figure 5. Recombination in the *attL-attR* substrate in the presence of integrase plus gp3. The assays were performed using the same substrate as in Figure 3. Integrase plus gp3 were added simultaneously, and the BM amplitude changes in individual molecules were followed. The data are assembled as in Figures 3 and 4.

of *attB* × *attP* recombination in the presence of integrase plus gp3 would not be inconsistent with prior biochemical results. The rate constants for the formation and dissociation of individual complexes were obtained from the relevant dwell times (Figure 6B and C; Table 2).

The above results demonstrate that inhibition of *attB-attP* recombination by gp3 is mediated through its interaction with integrase rather than its direct interaction with these *att* sites. The gp3-integrase interaction might precede or follow the binding of integrase to DNA. Synapsis *per se* of *attB-attP* sites is not impeded by gp3, rather the synapsed molecules are trapped in an abortive state in the presence of gp3 (Figure 6D).

Integrase-mediated inversion between *attB* and *attP*

The integrase is insensitive to the orientation of the *att* sites, and mediates efficient recombination when *attB-attP* or *attL-attR* are arranged in a head-to-head fashion. The DNA between the *att* sites is inverted as a result of the reaction; however, there is no net change in DNA length between substrate and product. Hence TPM cannot identify recombination events, and thus cannot distinguish between RS-complexes and WS-complexes. To follow the events ensuing integrase association with head-to-head oriented *attB-attP*, we employed a 1303 bp substrate analogous to those employed in prior experiments. Although the *attB* orientation with respect to *attP* was reversed in this substrate,

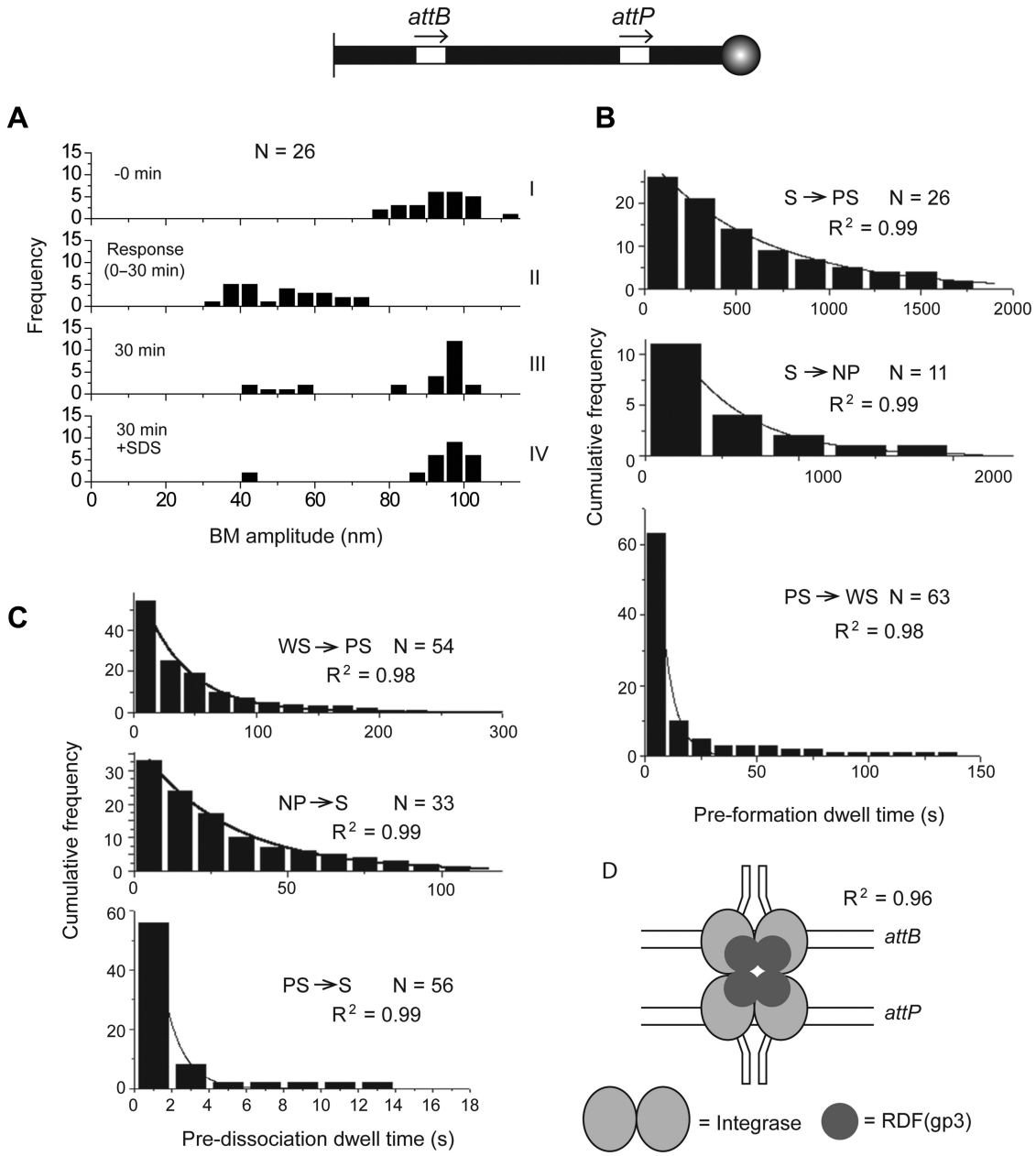

Figure 6. Effect of gp3 on integrase-mediated *attP-attB* recombination. The *attB-attP* substrate used for the analyses in Figure 3 was treated with integrase plus gp3. (**A**–**C**) Changes in the BM amplitude distributions following the addition of integrase plus gp3 and the dwell times relevant to the formation and dissociation of individual complexes are arranged as in Figures 3–5. The PS-complexes progressed to WS-complexes, consistent with the block in recombination. (**D**) A possible inactive conformation of the *attB-attP* synapse promoted by integrase plus gp3 is schematically shown. In this conformation, the interaction of the CCs is between integrase monomers bound to the same *att* site (see also Figure 1B). The integrase, its CC motifs and gp3 (ϕC31 RDF) are represented as in Figure 1B.

the 752 bp spacing between the sites was maintained as before.

The decrease in BM amplitude distribution upon integrase addition to DNA (in 30 out of 76 molecules) was consistent with the formation of integrase-bound molecules, unsynapsed as well as synapsed (Figure 7A-I–III). At 30 min, a large subset of the bound molecules shifted back to high amplitude due to decay of NP- and WS-complexes or having completed recombination (Figure 7A-III). Following SDS treatment, all but one oddly behaved molecule (perhaps stuck to the glass surface) exhibited the same amplitude as the substrate DNA (Figure 7A-IV). The rate constants based on the measured dwell times (Figure 7B and C) are summarized in (Table 2). As WS- and RS-complexes were indistinguishable in the *attB-attP* inversion system, the dwell times in the PS state were fit to a double exponential model to obtain two rate constants, one for the PS → RS conversion and the other for the PS → WS conversion (Figure 7B, bottom panel; Table 2).

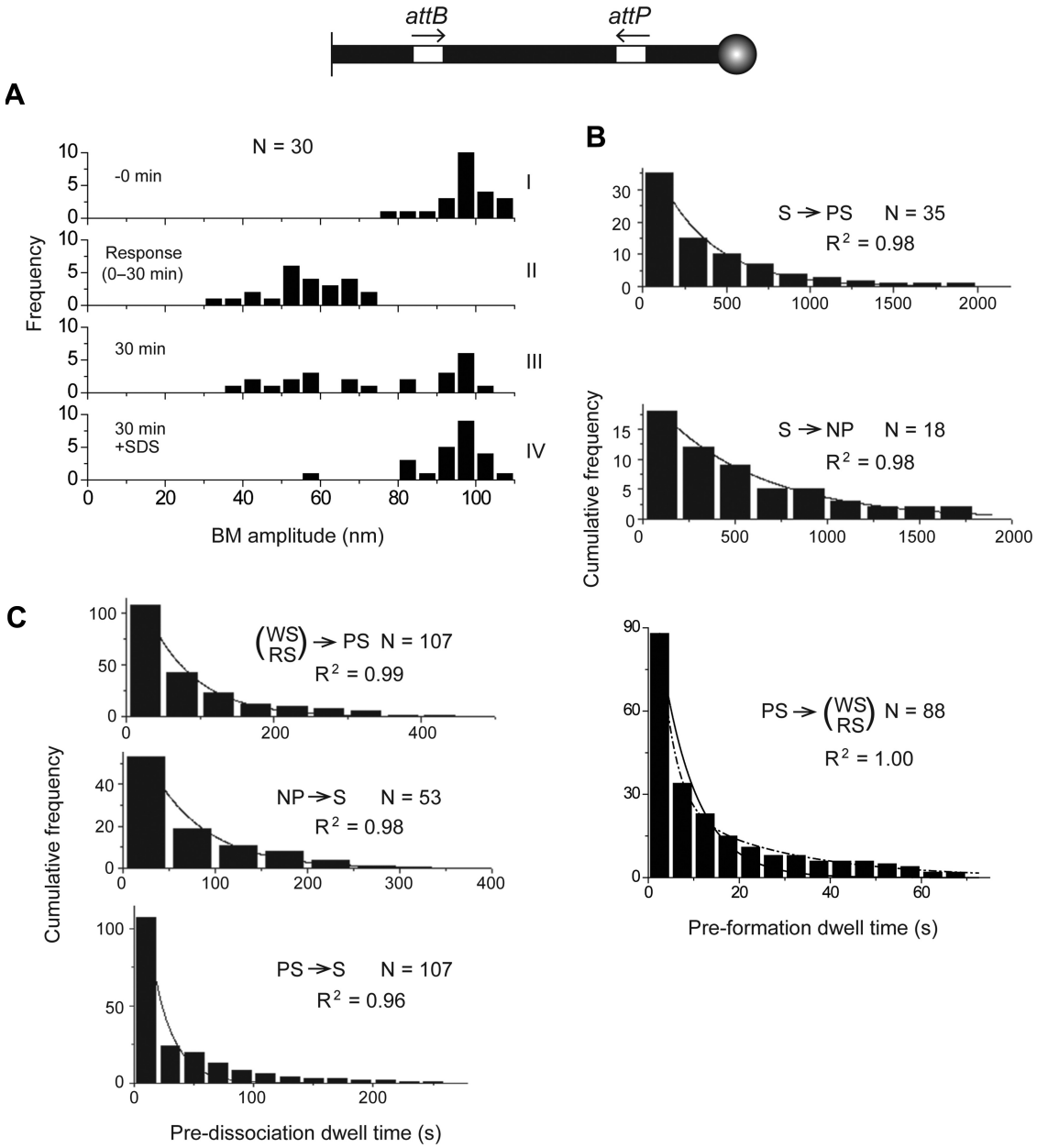

Figure 7. BM amplitude changes induced by integrase in an *attB-attP* head-to-head substrate. The substrate used for this assay differed from the one depicted in Figures 3 and 6 only in having the *attB-attP* sites in head-to-head orientation. The length of the substrate and the spacing between the sites were not changed. (**A**) The BM amplitude distributions and (**B** and **C**) the dwell time histograms are depicted as in Figure 3–6. In this assay, the dissociation of the WS-complex or completion of recombination (from the RS-complex) could not be distinguished, as the shift-up in BM amplitude is the same for both processes. The single exponential fit to the dwell times of the WS- and RS-complexes combined suggests that k-WS_d = k_{rec} = 1.5 ± 0.1 × 10^{-2} s^{-1}, k-WS_d = the rate constant for WS → PS dissociation and k_{rec} = the rate constant for recombination (Table 2). Similarly, the PS → RS and PS → WS steps were indistinguishable. The dwell times in the PS state, by a double exponential fit, gave k-RS_f = 2.5 ± 0.3 × 10^{-1} s^{-1} (PS → RS) and k-WS_f = 3.3 ± 0.4 × 10^{-2} s^{-1} (PS →WS), respectively (Table 2).

The TPM behavior of the head-to-head *attB-attP* sites are in overall agreement with results from biochemical assays demonstrating the recombination competence of *att* sites in various configurations, intramolecular or intermolecular (20,21,32,34,35,39). In principle, the fluctuations between the low amplitude synapsed state and the intermediate amplitude de-synapsed state must be composed of two kinetic components. One is the dissociation of WS-complexes and the other is authentic recombination from RS-complexes. However, the dwell times correspond to a single first order rate constant = (1.5 ± 0.1) × 10^{-2} s^{-1} (Table 2). Presumably the dissociation of the wayward substrate synapse and the recombinant product synapse occur with similar rate constants, and cannot be deconvoluted from the dwell times. Comparison of the rate constants of the individual reaction steps suggests that the dissociation of the product synapse represents the rate limiting step in the reaction pathway.

BM amplitude analyses of synaptic and wayward complexes

The well-studied transposon resolvases and bacterial or phage invertases have strict topological requirements, catalyze intramolecular reactions almost exclusively and are highly selective with respect to site orientation (2,3,42). By contrast, these rules do not apply to ϕC31 integrase or Bxb1 integrase (15,34,43,44). For example, these integrases can arrange *attB* and *attP* sites in parallel or anti-parallel fashion within a catalytically competent synaptic complex. Recombination is proscribed between sites in the anti-parallel geometry because of the asymmetry of the central 2-bp bordered by the scissile phosphates. In this arrangement, 180° rotation of the cleaved complex will generate mismatched bases at the center, inhibiting strand joining. An additional 180° rotation will restore complementarity and promote strand joining to yield the parental configuration.

As differences in synaptic architecture can cause changes in the effective length of DNA, TPM is capable of revealing alternative conformations of the synapse and/or alternative site alignments within the synaptic complex. In our earlier analysis of tyrosine recombinases, we noticed that the entry and exit points of DNA with respect to the synapsed sites influences the BM amplitude of the attached bead by a small but measurable amount (27,28) (Figure 8). When the entry and exit points are at the same end of the synapse (proximal), the tethered DNA behaves as if it were slightly shorter (more constrained) than when they are at opposite ends of the synapse. Consistent with the anti-parallel geometry of the tyrosine recombination synapse, the BM amplitude of synapsed molecules was slightly smaller for the head-to-tail orientation of target sites than for their head-to-head orientation. Although structural data on the synaptic organization of serine integrases are currently lacking, the models proposed by Rutherford and Van Duyne (36) based on the synaptic structures of other serine recombinases are helpful in relating measured BM amplitude values to potential synaptic configurations. We now probed the successfully synapsed RS-complexes and abortively synapsed WS-complexes formed in the *attB-attP* and *attL-attR* reactions for differences in their BM amplitudes.

For *attB-attP* sites in head-to-tail orientation, the mean BM amplitude of the RS-complexes was 42.5 ± 5.8 nm (Figure 8A). In conformity with biochemical and topological data, we assume that these complexes contained the sites in parallel geometry. The inactive WS-complexes (that did not produce recombinants) had a higher mean BM amplitude, 46.0 ± 7.5 nm (Figure 8B). They likely represent complexes in which the inter-monomer integrase interactions were not conducive to recombination. Such complexes may need to dissociate before they can be reconfigured to form a functional synapse. BM amplitudes lower than that of the RS-complexes seen at the tail end of this distribution may indicate synaptic complexes containing *attB* and *attP* in antiparallel geometry. Such complexes are expected to be catalytically competent but not recombinationally active. Despite two (or even) rounds of strand exchange catalyzed by them, their return to the substrate BM amplitude upon SDS challenge would categorize them as WS-complexes in our assay. We do not have a good explanation for the apparent paucity of the anti-parallel synapse, as earlier biochemical results would suggest equal abundance of parallel and anti-parallel *attB-attP* synapses. Perhaps the protein–DNA dynamics and/or allosteric interactions within synapsed molecules induce overlapping conformations that make the clean distinction between synapse geometries by BM amplitudes difficult.

The RS-complexes formed by head-to-tail *attL-attR* sites in the presence of integrase and gp3 gave a mean BM amplitude of 46.5 ± 5.0 nm (Figure 8C). As was noted for the head-to-tail *attB-attP* sites, the mean BM amplitude for the *attL-attR* WS-complexes was higher, 51.0 ± 5.4 nm (Figure 8D). However, the absence of complexes with a lower BM amplitude than the RS complexes was consistent with the gp3 protein, in collaboration with the integrase, precluding *attL-attR* alignment in the incorrect geometry. Dissociation of the WS-complexes may be a pre-requisite for correcting the non-functional conformation of the integrase tetramer associated with *attL-attR* (the likely cause for their higher BM amplitude).

The WS-complexes assembled by head-to-tail *attB-attP* in the presence of integrase and gp3 followed two overlapping Gaussian distributions, with mean BM amplitudes of 41.1 ± 5.7 nm and 54.3 ± 3.3 nm (Figure 8E; Table 3). An analogous two-Gaussian pattern accounted for the WS-complexes formed as a result of *attL-attR* synapsis by integrase in the absence of gp3. The corresponding BM amplitudes were 44.1 ± 4.9 nm and 56.0 ± 3.9 nm (Figure 8F; Table 3). The lower and higher BM amplitudes of the two WS-subpopulations differ by nearly the same amount (12–13 nm) for the *attB-attP* and the *attL-attR* sites. Furthermore, for each subpopulation, the value is slightly higher (2–3 nm) for the *attL-attR* substrate (Table 3). These results suggest that the presence of gp3 in the case of *attB-attP* and its absence in the case of *attL-attR* promote analogous inactive conformations in the synaptic complexes formed by these sites. The inactive state may be induced by allosteric changes in protein conformations, altered DNA–protein interactions that spawn non-productive site alignments or by aberrant protein–DNA dynamics within the synapse. The TPM assay is not sensitive enough to pinpoint or resolve these potential contributing factors. Interestingly, even under recombination-proficient reactions (*attB-attP* with integrase; *attL-attR* with integrase plus gp3), the RS- and WS-complexes formed by *attL-attR* have a slightly higher BM amplitude (4–5 nm) than their respective counterparts formed by *attB-attP* (Table 3).

Collectively, the TPM results suggest that the recombination-competent and recombination-incompetent conformations of *attB-attP* and *attL-attR* synapses can be distinguished by their distinct BM amplitudes. In the present structural view (36), one mode of interactions within the integrase tetramer fosters functional synapsis in *attB-attP* as well as *attL-attR* (Figure 1B). An alternative mode of interactions induces non-functional synapsis of the same partner sites (Figure 1B and Figure 6D). The BM amplitude distributions suggest more than one conformation (at least two) for the inactive synaptic complexes generated by *attB-attP* pairing in the presence of gp3 and by *attL-attR* pairing in its absence.

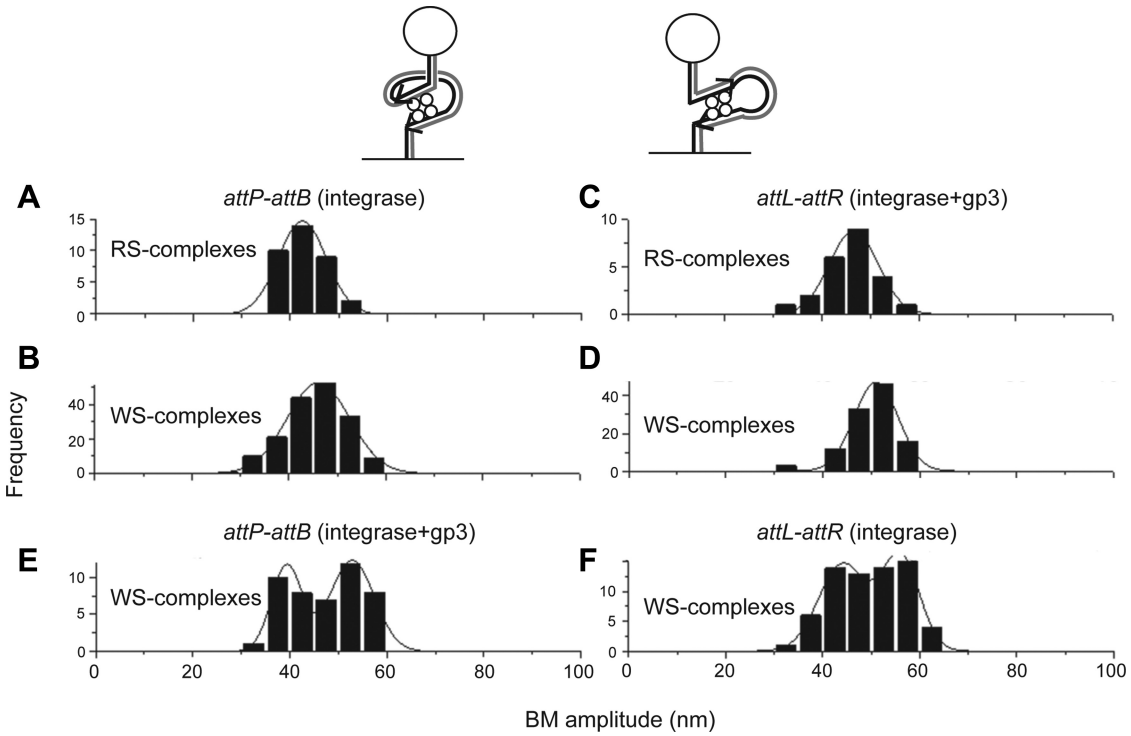

Figure 8. BM amplitude distributions of recombinationally active and inactive synapses formed by *attB-attP* and *attL-attR*. The parallel (left) and anti-parallel (right) synaptic geometries for two sites in head-to-tail orientation are schematically illustrated at the top. Previous studies with YRs suggested that the synaptic conformation at the right is slightly more constrained than that at the left, and thus has a lower BM amplitude. (**A**) The BM amplitude distribution for the RS-complexes (recombination-competent) from the head-to-tail *attB-attP* reaction with integrase had a mean = 42.5 ± 5.8 nm (N = 39). (**B**) The WS-complexes in the same reaction formed a distribution with a mean BM amplitude of 46.0 ± 7.5 nm (N = 170). (**C**) The RS-complexes from the *attL-attR* reaction containing integrase plus gp3 showed a mean BM amplitude of 46.5 ± 5.0 nm (N = 23). (**D**) The corresponding value for the WS-complexes in the same reaction was 51.4 ± 5.4 nm (N = 110). (**E**) In the presence of integrase plus gp3, the WS-complexes assembled by the head-to-tail *attP-attB* substrate conformed to a bimodal distribution with mean BM amplitudes of 41.1 ± 5.7 nm and 54.3 ± 3.3 nm (N = 46). (**F**) Integrase, in the absence of gp3, induced an analogous distribution of WS-complexes in the head-to-tail *attL-attR* substrate. The mean BM amplitudes were 44.1 ± 4.9 nm and 56.0 ± 3.9 nm (N = 67).

Table 3. BM amplitudes of *attB-attP* and *attL-attR* synaptic complexes under conditions that are permissive or non-permissive for recombination. The data from Figure 8 for the BM amplitudes of RS- and WS-complexes are tabulated

	BM amplitude of synapse (nm)	
Substrate	Recombination-Proficient	Recombination-blocked
(→〰→) *attB-attP*	Integrase	Integrase + gp3
	RS: 42.5 ± 5.8; WS: 46.0 ± 7.5	WS: 41.1 ± 5.7 ; 54.3 ± 3.3
(→〰→) *attL-attR*	Integrase + gp3	Integrase
	RS: 46.5 ± 5.0; WS: 51.0 ± 5.4	WS: 44.1 ± 4.9 ; 56.0 ± 3.9

Rotational freedom and life-time of the cleaved recombination complex

A recombinant outcome during the action of a serine recombinase requires that the relative rotation of the cleaved recombinase-associated DNA be regulated, ensuring that strand joining occurs at 180° rotation. An additional 180° rotation or multiples of 360° rotation before strand joining would result in a futile reaction. In the case of the small serine recombinases (resolvases and invertases), substrate supercoiling and accessory DNA–protein interactions specify a defined synapse topology, parallel orientation of partner sites and chiral rotation of the cleaved DNA through 180° to promote strand joining in the recombinant mode (2,3,42). Certain 'activating' mutations, when harbored by a recombinase, can free it from the constraints of DNA topology and accessory DNA–protein interactions (45–47). Such activated variants violate the rules of a unique synapse, a fixed geometry of site alignment and a single round of 180° rotation.

The large serine recombinases, ϕC31 and Bxb1 integrases, resemble activated small serine recombinases in their disregard for substrate and synapse topologies and in their ability to mediate strand exchange between *attB* and *attP* sites paired in parallel or anti-parallel geometry (34,44). Are the phage integrases then also unrestrained in the rotation of the cleaved DNA within the recombination synapse? At present the answer is ambiguous. Experimental observations for the Bxb1 integrase suggest a long life-time for the cleaved complex and free DNA rotation (31). However, results with ϕC31 integrase support gated rotation, favoring strand joining that produces recombinants (32). The TPM data from substrate–protein combinations that promote chemically competent synaptic complexes can provide indirect evidence that favors one model or the other.

The free rotation model predicts a significant steady state level of the cleaved DNA among actively recombining substrate molecules. Indeed, an activated variant of the Sin resolvase from *Staphylococcus aureus* is more active in strand cleavage than wild-type Sin (47). The TPM assays included three recombination-competent conditions: head-to-tail or head-to-head *attB-attP* treated with integrase and head-to-tail *attL-attR* treated with integrase plus gp3. In a substrate molecule containing double strand cleavage at one or both *att* sites, the tethered DNA segment will be separated from the bead when SDS is added to the reaction mixture (Figure 9A). However, analysis of the molecules that formed bound complexes with integrase or integrase plus gp3 gave no indication of SDS-mediated bead separation. By contrast, treatment of the head-to-tail *attB-attP* substrate with Sal I restriction enzyme in the TPM set up caused the release of the beads from nearly all of the molecules (even in the absence of SDS treatment) (Figure 9B).

The absence or rarity of unsealed cleavages in the *att* sites under conditions that promote recombination is consistent with the gated rotation model for ϕC31 integrase, as was proposed earlier (32).

DISCUSSION

The present stepwise analysis of the recombination reaction mediated by ϕC31integrase brings to light thermodynamic and kinetic features of the reaction beyond those gleaned from previous ensemble biochemical investigations. The conclusions reached from the single-molecule TPM assays, which are in general agreement with the current structural and mechanistic understanding of the system, are summarized in Figure 10 and Table 2. The productive reaction path begins with the binding of integrase to *attB-attP* or integrase plus gp3 to *attL-attR* to form the PS-complex. The PS-complex is the precursor of the RS-complex, in which the *att* sites are paired to form a functional synapse. The chemical steps of stand cleavage and strand joining within the RS-complex, interposed by the conformational dynamics of DNA rotation, complete recombination. The transience of the cleaved DNA intermediate is consistent with a gated rotation of 180° between the cleavage and joining events.

The abortive off-pathway complexes revealed by TPM are protein–DNA associations that fail to proceed to synapsis (NP-complexes) or synapsed molecules that fail at recombination (WS-complexes). However, these complexes do get second chances at recombination by reverting to the pre-synaptic state (WS → PS) or returning to the substrate (NP →S; WS → PS → S) and starting over (Figure 10).

Thermodynamic aspects of integrative and excisive recombination by integrase

Under the single-molecule assay conditions with head-to-tail sites, protein association occurs in ∼58% of *attB-attP* containing molecules in the presence of integrase and in ∼45% of *attL-attR* containing molecules in the presence of integrase plus gp3 (Figure 10). The bound fraction decreases to ∼23% for *attB-attP* with integrase plus gp3 and to ∼27% for *attL-attR* with integrase alone. The fraction of head-to-head *attB-attP* sites bound by integrase (*sans* gp3) is ∼40%. Thus, conditions that confer recombination competence on the *att* site pair appear to promote the initial step of integrase or integrase plus gp3 binding to DNA. Presumably, the interactions between gp3 and integrase in solution thermodynamically favors integrase binding to *attL* and *attR* while exerting the opposite effect on *attB* and *attP* sites. Thus, gp3 appears to promote or block the commitment to recombination at the earliest pre-chemical step of the reaction.

In the presence of integrase plus gp3, the bound *attL-attR* complexes are partitioned predominantly toward synapsis as against protein dissociation (∼86% PS- and ∼14% NP-complexes) (Figure 10). With integrase alone, the fractions are ∼55% PS- and ∼45% NP-complexes. The *attB-attP* sites do not show a striking differential response to integrase (∼93% PS- and ∼7% NP-complexes) versus integrase plus gp3 (∼88.5% PS- and ∼11.5% NP-complexes) (Figure 10). Under recombination-conducive conditions, the functionally synapsed molecules are slightly lower than the abortive ones for the *attB-attP* sites (∼53.5% WS- and ∼46.5% RS-complexes) as well as the *attL-attR* sites (∼52% WS- and ∼48% RS-complexes) (Figure 10). The marked reduction in the yield of *attL-attR* PS-complexes without gp3 (from ∼86% to ∼55%) is consistent with the notion that formation of the synapse is a critical regulatory step in determining the directionality of recombination (21,43). However, in

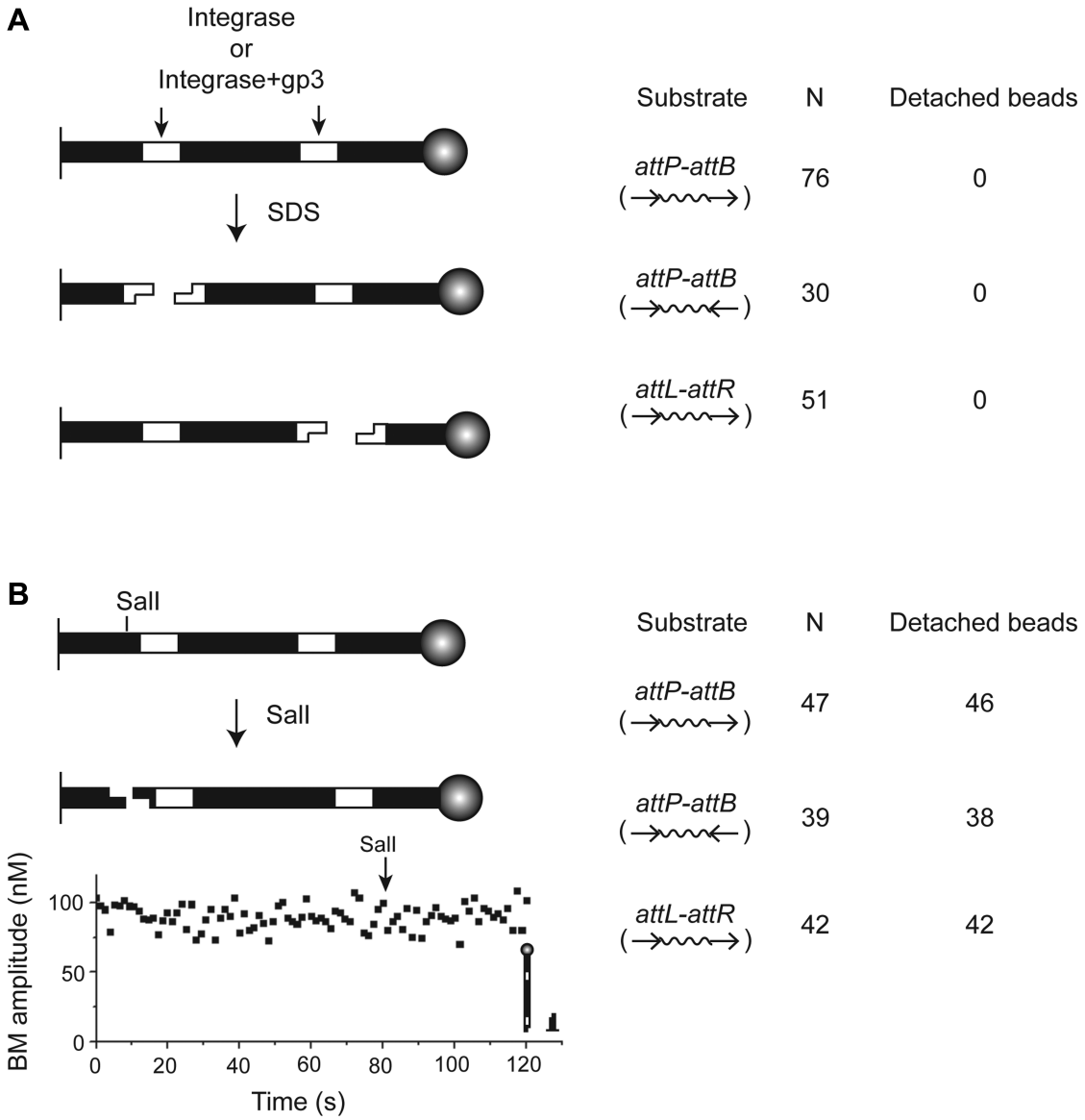

Figure 9. Bead separation from the tethered DNA substrate containing *attB-attP* by addition of SalI. (**A**) In the schematic representation of the 1303 bp recombination substrates (containing *attB-attP* or *attL-attR*), the integrase cleavage sites are indicated by the short vertical arrows. The vertical line at the left and the sphere at the right indicate the tethering glass surface and the polystyrene bead, respectively. Double strand cleavage at one or both *att* sites will result in bead detachment from the tethered DNA. The number of molecules with detached beads following SDS treatment from three assays are tabulated. The orientation of the *att* sites in a substrate is indicated by the arrows. The *attB-attP* reactions contained integrase. The *attL-attR* reaction contained integrase plus gp3. (**B**) In the 1303 bp DNA substrate with head-to-tail *attB-attP* sites, the SalI recognition site located 241 bp away from the end attached to the glass surface. SalI digestion would release the bead along with the long DNA fragment from the short fragment that remains tethered. The BM amplitude time trace of a molecule before and after SalI addition (indicated by the short vertical arrow) are shown. The abrupt termination of the trace resulted from bead detachment. Such events from three separate experiments are tabulated. N refers to the number of DNA molecules observed.

contrast to the earlier biochemical results, the TPM findings reveal that *attL-attR* synapsis is not abolished by the lack of gp3. Furthermore, gp3 has little effect on the extent of synapsis of *attB-attP* sites (∼93%% and ∼89% in its presence and absence, respectively). Our data suggest that gp3 controls *attL-attR* recombination at the level of both synapse formation and synapse architecture. It controls *attB-attP* recombination almost exclusively at the level of synaptic architecture. Additional nuances on synaptic conformations and recombination directionality are considered in a separate section (see below).

Kinetic features of recombination by integrase

The rate constants for the formation of integrase- or integrase plus gp3-bound *att* site complexes are in the 10^5–10^6 M^{-1} s^{-1} range, the maximum difference among the *att* site pairs being ∼5-fold (Table 2). For a given *att* site pair-protein combination, the NP- and PS-complexes are generated with similar kinetics (<2-fold difference). Under conditions permissive for recombination (*attB-attP*, integrase; *attL-attR*, integrase plus gp3), head-to-tail *attB-attP* sites form RS-complexes (functional synapsis) ∼10-fold faster

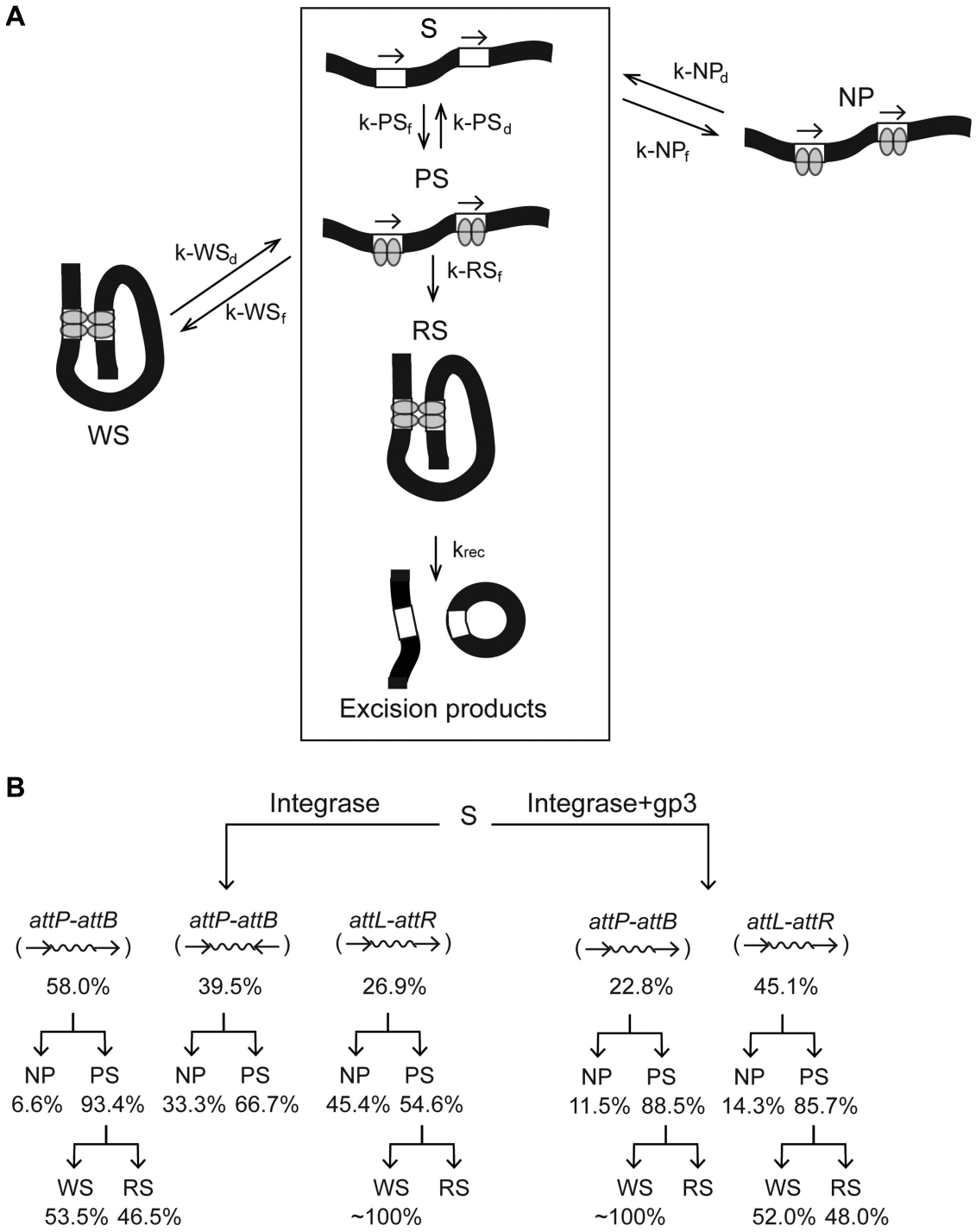

Figure 10. The pathway for ϕC31 integrase-mediated recombination deduced from the TPM assays. The scheme at the top summarizes the excision reaction between head-to-tail *attB-attP* sites catalyzed by integrase and that between head-to-tail *attL-attR* sites catalyzed by integrase plus gp3. The individual complexes are described in the text as well as in Figure 2 and Table 1. The productive reaction path is enclosed within the rectangular box. The complexes outside the box (off-pathway complexes) can enter the productive path via conversion to the pre-synaptic complex (PS) or to the substrate (S). In the *attB-attP* reaction with integrase plus gp3 and in the *attL-attR* reaction with integrase alone, the synapsis to recombination step is blocked or strongly impeded. The values for the indicated kinetic constants are summarized in Table 2. The cumulative results on *att* site interactions with integrase or integrase plus gp3 (Figures 3–7) are summarized below.

than head-to-tail *attL-attR* sites (6.3×10^{-1} s^{-1} versus 6.6×10^{-2} s^{-1}). The opposite is observed for abortive synapsis under these conditions, the *attL-attR* sites forming WS-complexes approximately six times faster than the *attB-attP* sites (4.6×10^{-1} s^{-1} versus 7.2×10^{-2} s^{-1}). The WS- and NP-complexes formed by the different partner sites dissociate (WS → PS; NP → S) with rate constants that vary within a ∼5-fold range (1.4×10^{-2} s^{-1} to 6.5×10^{-2} s^{-1}). A subset of the PS complexes formed by de-synapsis of WS-complexes dissociate (PS → S) quite rapidly (1.3×10^{-1} s^{-1} to 9.1×10^{-1} s^{-1}) compared to the NP complexes. Thus, the WS → S and NP → S conversions are overall similar in their kinetics. The rate constant for recombination, inferred indirectly from the head-to-head *attB-attP* reaction with integrase, is of the same order as the dissociation of the WS-complexes and the NP complexes.

The association kinetics of integrase or integrase plus gp3 with the *att* sites are generally comparable to those of the YRs Cre and Flp with their respective target sites, measured in analogous TPM assays (25,27). In the presence of integrase plus the gp3 protein, synapsis by head-to-tail *attB-attP* is channeled toward WS-complexes at the expense of RS-complexes. However, there is little difference (<∼2-fold) in the kinetics of this step, whether it is mediated by integrase or integrase plus gp3. The production of RS-complexes by head-to-tail *attL-attR* is triggered only in the presence of integrase plus gp3, albeit with a ∼10-fold lower rate constant than that for functional synapsis by head-to-tail *attB-attP* bound by integrase. At the same time, gp3 also accelerates the formation of WS-complexes by *attL-attR* (∼15-fold increase in the rate constant over that with integrase alone). While the integrase plus gp3 combination boosts functional *attL-attR* synapsis thermodynamically, kinetically it favors abortive synapsis. Among potential alternative modes of *attL-attR* pairing, WS-complexes are likely less constrained structurally than RS-complexes, and are therefore produced faster. When the RS- and WS-complexes are pooled as synapsed molecules (by disregarding their functional status), the kinetics of *attB-attP* synapsis by integrase alone and the kinetics of *attL-attR* synapsis by integrase plus gp3 become comparable. As dissociation of the WS- and NP-complexes follow similar kinetics as recombination, they have the opportunity to reattempt recombination via PS → RS or S → PS →RS conversions. The kinetic data are consistent with the rate limiting step in recombination (RS → products) being the dissociation of the synapse holding together the product *att* sites.

DNA and protein contributions to synaptic architecture and recombination directionality

The phage integrase systems are characterized by strict selectivity of *att* site partners and the uni-directionality of the recombination reaction. These features are controlled by distinct DNA–protein conformations resulting from integrase binding to a P-type half-site (P or P′) versus a B-type half-site (B or B′) (Figure 1C), inter-monomer interactions within and between integrase dimers associated with each of the two *att* sites and modulations of these interactions by the RDF proteins (15,36,43,44,48). In addition, the central dinucleotide extension in the cleaved DNA determines whether strand joining will occur after 180° rotation (in the recombinant mode) or after an additional 180° rotation (in the parental mode) (43,44). The *attB* and *attP* sites are quasi-symmetric (P-P′; B-B′), while *attL* and *attR* (the products of *attB* x *attP*) are asymmetric (B-P′; P-B′). Biochemical and topological studies (43,44,49), in particular in the Bxb1 integrase system, reveals the following rules that govern synaptic compatibility of a pair of *att* sites. Functional synapsis requires two interactions, each between an integrase monomer associated with a B-type half-site (B or B′) and one associated with a P-type half-site (P or P′). Within a chemically competent synapse, the asymmetry of the central dinucleotide directs recombination to a physiologically meaningful outcome. In accordance with the first rule, *attB-attB* or *attP-attP* synapsis is proscribed, while *attB-attP* synapsis may occur with the sites in parallel or anti-parallel geometry. Similarly, *attL-attR* (parallel), *attL-attL* (anti-parallel) and *attR-attR* (anti-parallel) synapses are permissible. However, the second rule excludes recombination in all but parallel synapses formed by *attB-attP* and *attL-attR* sites. Finally, RDF promotes excisive recombination and inhibits integrative recombination, presumably by modulating inter-monomer integrase interactions.

The TPM assays complement and refine the current biochemical observations by demonstrating that synapsis *per se* of *att* sites does not necessarily commit them to recombination. Not all synaptic events under conditions that favor recombination are fruitful. In fact, WS-complexes slightly exceed RS-complexes in *attB-attP* reactions with integrase and *attL-attR* reactions with integrase plus gp3. The WS-complexes have a slightly higher BM amplitude than the RS-complexes. This apparent longer tether length in the WS-complexes suggests a less compact synapse. Under recombination-blocked conditions, *attB-attP* and *attL-attR* do not form RS-complexes but still generate WS-complexes. The two distinct BM amplitudes displayed by these complexes, for both *attB-attP* and *attL-attR*, may indicate synapsed molecules with alternative protein conformations and/or site alignments.

The importance of the C-terminal domain of ϕC31 integrase in forming a chemically competent synapse was predicted from the isolation of an activated integrase variant capable of performing *attL* × *attR*, *attL* × *attL* and *attR* × *attR* recombination in addition to *attB* × *attP* recombination (39). The mutation maps to the start of a potential coiled-coil motif (E449K), suggesting that the synaptic interfaces during integration and excision is controlled by inter-monomer interactions within the integrase tetramer. Current structural data, though limited, uphold this notion by highlighting the importance of structural motifs present in the C-terminal domain of the *Listeria* phage integrase, in particular interactions between the coiled-coil motifs of adjacent monomers bound to DNA, in determining whether the active sites are in a catalytically active or inactive state (36). Insights gained form the present TPM studies into the roles of wild-type ϕC31 integrase and the gp3 protein in regulating the pre-chemical steps of *attB* × *attP* or *attL* × *attR* recombination encourage similar analysis of the action of Int(E449K) and other activated integrase variants (39,48) on various *att* site combinations.

SUPPLEMENTARY DATA

Supplementary Data are available at NAR Online.

ACKNOWLEDGEMENTS

The authors are grateful to Margaret C. M. Smith and colleagues for the generous gift of the expression plasmids for PhiC31 integrase and the gp3 protein. The authors thank Paul A Rowley for critical reading of the manuscript.

FUNDING

Ministry Science and Technology, R.O.C.; Yang Ming University (HFF); Robert F Welch Foundation F-1274 [to M.J.]. Funding for open access charge: The Ministry Science and Technology, R.O.C. (MOST 105-2119-M-010-001).
Conflict of interest statement. None declared.

REFERENCES

1. Jayaram,M., Ma,C.H., Kachroo,A.H., Rowley,P.A., Guga,P., Fan,H.F. and Voziyanov,Y. (2015) An overview of tyrosine site-specific recombination: from a Flp perspective. In: Craig,NL, Chandler,M, Lambowitz,AM, Gellert,M, Rice,PA and Sandmeyer,S (eds). *Mobile DNA III*. ASM Press, Washington DC, pp. 43–71.
2. Stark,W.M. (2015) The Serine Recombinases. In: Craig,NL, Chandler,M, Lambowitz,AM, Gellert,M, Rice,PA and Sandmeyer,S (eds). *Mobile DNA III*. ASM Press, Washington DC, pp. 73–90.
3. Grindley,N.D., Whiteson,K.L. and Rice,P.A. (2006) Mechanisms of site-specific recombination. *Annu. Rev. Biochem.*, **75**, 567–605.
4. Brown,W.R., Lee,N.C., Xu,Z. and Smith,M.C. (2011) Serine recombinases as tools for genome engineering. *Methods*, **53**, 372–379.
5. Chavez,C.L. and Calos,M.P. (2011) Therapeutic applications of the φC31 integrase system. *Curr. Gene Ther.*, **11**, 375–381.
6. Garcia-Otin,A.L. and Guillou,F. (2006) Mammalian genome targeting using site-specific recombinases. *Front. Biosci.*, **11**, 1108–1136.
7. Olorunniji,F.J., Rosser,S.J. and Stark,W.M. (2016) Site-specific recombinases: molecular machines for the genetic revolution. *Biochem. J.*, **473**, 673–684.
8. Turan,S., Galla,M., Ernst,E., Qiao,J., Voelkel,C., Schiedlmeier,B., Zehe,C. and Bode,J. (2011) Recombinase-mediated cassette exchange (RMCE): Traditional concepts and current challenges. *J. Mol. Biol.*, **407**, 193–221.
9. Dhar,G., Sanders,E.R. and Johnson,R.C. (2004) Architecture of the Hin synaptic complex during recombination: the recombinase subunits translocate with the DNA strands. *Cell*, **119**, 33–45.
10. Kamtekar,S., Ho,R.S., Cocco,M.J., Li,W., Wenwieser,S.V., Boocock,M.R., Grindley,N.D. and Steitz,T.A. (2006) Implications of structures of synaptic tetramers of γδ resolvase for the mechanism of recombination. *Proc. Natl. Acad. Sci. U.S.A.*, **103**, 10642–10647.
11. Kanaar,R., Klippel,A., Shekhtman,E., Dungan,J.M., Kahmann,R. and Cozzarelli,N.R. (1990) Processive recombination by the phage Mu Gin system: Implications for the mechanisms of DNA strand exchange, DNA site alignment, and enhancer action. *Cell*, **62**, 353–366.
12. Stark,W.M., Sherratt,D.J. and Boocock,M.R. (1989) Site-specific recombination by Tn3 resolvase: topological changes in the forward and reverse reactions. *Cell*, **58**, 779–790.
13. Wasserman,S.A., Dungan,J.M. and Cozzarelli,N.R. (1985) Discovery of a predicted DNA knot substantiates a model for site-specific recombination. *Science*, **229**, 171–174.
14. Van Duyne,G.D. (2015) Cre Recombinase. In: Craig,NL, Chandler,M, Lambowitz,AM, Gellert,M, Rice,PA and Sandmeyer,S (eds). *Mobile DNA III*. ASM Press, Washington DC, pp. 119–138.
15. Smith,M.C., Brown,W.R., McEwan,A.R. and Rowley,P.A. (2010) Site-specific recombination by φC31 integrase and other large serine recombinases. *Biochem. Soc. Trans.*, **38**, 388–394.
16. Van Duyne,G.D. and Rutherford,K. (2013) Large serine recombinase domain structure and attachment site binding. *Crit. Rev. Biochem. Mol. Biol.*, **48**, 476–491.
17. Kim,A.I., Ghosh,P., Aaron,M.A., Bibb,L.A., Jain,S. and Hatfull,G.F. (2003) Mycobacteriophage Bxb1 integrates into the Mycobacterium smegmatis groEL1 gene. *Mol. Microbiol.*, **50**, 463–473.
18. Landy,A. (2015) The lambda integrase site-specific recombination pathway. In: Craig,NL, Chandler,M, Lambowitz,AM, Gellert,M, Rice,PA and Sandmeyer,S (eds). *Mobile DNA III*. ASM Press, Washington DC, pp. 91–118.
19. Smith,M.C. and Thorpe,H.M. (2002) Diversity in the serine recombinases. *Mol. Microbiol.*, **44**, 299–307.
20. Thorpe,H.M. and Smith,M.C. (1998) In vitro site-specific integration of bacteriophage DNA catalyzed by a recombinase of the resolvase/invertase family. *Proc. Natl. Acad. Sci. U.S.A.*, **95**, 5505–5510.
21. Khaleel,T., Younger,E., McEwan,A.R., Varghese,A.S. and Smith,M.C. (2011) A phage protein that binds φC31 integrase to switch its directionality. *Mol. Microbiol.*, **80**, 1450–1463.
22. Bibb,L.A., Hancox,M.I. and Hatfull,G.F. (2005) Integration and excision by the large serine recombinase φRv1 integrase. *Mol. Microbiol.*, **55**, 1896–1910.
23. Ghosh,P., Wasil,L.R. and Hatfull,G.F. (2006) Control of phage Bxb1 excision by a novel recombination directionality factor. *PLoS Biol.*, **4**, e186.
24. Zhang,L., Zhu,B., Dai,R., Zhao,G. and Ding,X. (2013) Control of directionality in Streptomyces phage φBT1 integrase-mediated site-specific recombination. *PLoS One*, **8**, e80434.
25. Fan,H.F. (2012) Real-time single-molecule tethered particle motion experiments reveal the kinetics and mechanisms of Cre-mediated site-specific recombination. *Nucleic Acids Res.*, **40**, 6208–6222.
26. Fan,H.F., Cheng,Y.S., Ma,C.H. and Jayaram,M. (2015) Single molecule TPM analysis of the catalytic pentad mutants of Cre and Flp site-specific recombinases: Contributions of the pentad residues to the pre-chemical steps of recombination. *Nucleic Acids Res.*, **43**, 3237–3255.
27. Fan,H.F., Ma,C.H. and Jayaram,M. (2013) Real-time single-molecule tethered particle motion analysis reveals mechanistic similarities and contrasts of Flp site-specific recombinase with Cre and lambda Int. *Nucleic Acids Res.*, **41**, 7031–7047.
28. Ma,C.H., Liu,Y.T., Savva,C.G., Rowley,P.A., Cannon,B., Fan,H.F., Russell,R., Holzenburg,A. and Jayaram,M. (2014) Organization of DNA partners and strand exchange mechanisms during Flp site-specific recombination analyzed by difference topology, single molecule FRET and single molecule TPM. *J. Mol. Biol.*, **426**, 793–815.
29. Mumm,J.P., Landy,A. and Gelles,J. (2006) Viewing single λ site-specific recombination events from start to finish. *EMBO J.*, **25**, 4586–4595.
30. Pinkney,J.N., Zawadzki,P., Mazuryk,J., Arciszewska,L.K., Sherratt,D.J. and Kapanidis,A.N. (2012) Capturing reaction paths and intermediates in Cre-loxP recombination using single-molecule fluorescence. *Proc. Natl. Acad. Sci. U.S.A.*, **109**, 20871–20876.
31. Bai,H., Sun,M., Ghosh,P., Hatfull,G.F., Grindley,N.D. and Marko,J.F. (2011) Single-molecule analysis reveals the molecular bearing mechanism of DNA strand exchange by a serine recombinase. *Proc. Natl. Acad. Sci. U.S.A.*, **108**, 7419–7424.
32. Olorunniji,F.J., Buck,D.E., Colloms,S.D., McEwan,A.R., Smith,M.C., Stark,W.M. and Rosser,S.J. (2012) Gated rotation mechanism of site-specific recombination by φC31 integrase. *Proc. Natl. Acad. Sci. U.S.A.*, **109**, 19661–19666.
33. Ghosh,P., Pannunzio,N.R. and Hatfull,G.F. (2005) Synapsis in phage Bxb1 integration: selection mechanism for the correct pair of recombination sites. *J. Mol. Biol.*, **349**, 331–348.
34. Smith,M.C., Till,R., Brady,K., Soultanas,P., Thorpe,H. and Smith,M.C. (2004) Synapsis and DNA cleavage in φC31 integrase-mediated site-specific recombination. *Nucleic Acids Res.*, **32**, 2607–2617.
35. Thorpe,H.M., Wilson,S.E. and Smith,M.C. (2000) Control of directionality in the site-specific recombination system of the Streptomyces phage φC31. *Mol. Microbiol.*, **38**, 232–241.

36. Rutherford,K., Yuan,P., Perry,K., Sharp,R. and Van Duyne,G.D. (2013) Attachment site recognition and regulation of directionality by the serine integrases. *Nucleic Acids Res.*, **41**, 8341–8356.
37. Gupta,M., Till,R. and Smith,M.C. (2007) Sequences in attB that affect the ability of φC31 integrase to synapse and to activate DNA cleavage. *Nucleic Acids Res.*, **35**, 3407–3419.
38. Liu,S., Ma,J., Wang,W., Zhang,M., Xin,Q., Peng,S., Li,R. and Zhu,H. (2010) Mutational analysis of highly conserved residues in the phage φC31 integrase reveals key amino acids necessary for the DNA recombination. *PLoS One*, **5**, e8863.
39. Rowley,P.A., Smith,M.C., Younger,E. and Smith,M.C. (2008) A motif in the C-terminal domain of φC31 integrase controls the directionality of recombination. *Nucleic Acids Res.*, **36**, 3879–3891.
40. Fan,H.F., Cox,M.M. and Li,H.W. (2011) Developing single-molecule TPM experiments for direct observation of successful RecA-mediated strand exchange reaction. *PLoS One*, **6**, e21359.
41. McEwan,A.R., Raab,A., Kelly,S.M., Feldmann,J. and Smith,M.C. (2011) Zinc is essential for high-affinity DNA binding and recombinase activity of PhiC31 integrase. *Nucleic Acids Res.*, **39**, 6137–6147.
42. Johnson,R. (2002) Bacterial site-specific DNA inversion systems. In: Craig,NL, Craigie,R, Gellert,M and Lambowitz,AM (eds). *Mobile DNA II*. ASM Press, Washington DC, pp. 230–271.
43. Ghosh,P., Bibb,L.A. and Hatfull,G.F. (2008) Two-step site selection for serine-integrase-mediated excision: DNA-directed integrase conformation and central dinucleotide proofreading. *Proc. Natl. Acad. Sci. U.S.A.*, **105**, 3238–3243.
44. Ghosh,P., Kim,A.I. and Hatfull,G.F. (2003) The orientation of mycobacteriophage Bxb1 integration is solely dependent on the central dinucleotide of attP and attB. *Mol. Cell*, **12**, 1101–1111.
45. Klippel,A., Kanaar,R., Kahmann,R. and Cozzarelli,N.R. (1993) Analysis of strand exchange and DNA binding of enhancer-independent Gin recombinase mutants. *EMBO J.*, **12**, 1047–1057.
46. Olorunniji,F.J., He,J., Wenwieser,S.V., Boocock,M.R. and Stark,W.M. (2008) Synapsis and catalysis by activated Tn3 resolvase mutants. *Nucleic Acids Res.*, **36**, 7181–7191.
47. Rowland,S.J., Boocock,M.R. and Stark,W.M. (2005) Regulation of Sin recombinase by accessory proteins. *Mol. Microbiol.*, **56**, 371–382.
48. McEwan,A.R., Rowley,P.A. and Smith,M.C. (2009) DNA binding and synapsis by the large C-terminal domain of φC31 integrase. *Nucleic Acids Res.*, **37**, 4764–4773.
49. Smith,M.C., Till,R. and Smith,M.C. (2004) Switching the polarity of a bacteriophage integration system. *Mol. Microbiol.*, **51**, 1719–1728.